UPCONVERTING NANOPARTICLES: SYNTHESIS, CHARACTERIZATION

AND BIOMEDICAL APPLICATION

Mr. Thapakorn Tree-udom

A Dissertation Submitted in Partial Fulfillment of the Requirements

for the Degree of Doctor of Philosophy Program in Nanoscience and Technology

(Interdisciplinary Program)

Graduate School

Chulalongkorn University

Academic Year 2015

Copyright of Chulalongkorn University

อนุภาคนาโนอัพคอนเวอร์ติง : การสังเคราะห์ พิสูจน์เอกลักษณ์ และการประยุกต์ใช้ทางชีวเวช

นายฐาปกรณ์ ตรีอุดม

Thesis Title	UPCONVERTING NANOPARTICLES: SYNTHESIS, CHARACTERIZATION AND BIOMEDICAL APPLICATION
By	Mr. Thapakorn Tree-udom
Field of Study	Nanoscience and Technology
Thesis Advisor	Associate Professor Supason Wanichwecharungruang, Ph.D.
Thesis Co-Advisor	Numpon Insin, Ph.D.

Accepted by the Graduate School, Chulalongkorn University in Partial Fulfillment of the Requirements for the Doctoral Degree

--Dean of the Graduate School

(Associate Professor Sunait Chutintaranond, Ph.D.)

THESIS COMMITTEE

--Chairman

(Associate Professor Vudhichai Parasuk, Ph.D.)

--Thesis Advisor

(Associate Professor Supason Wanichwecharungruang, Ph.D.)

--Thesis Co-Advisor

(Numpon Insin, Ph.D.)

--Examiner

(Associate Professor Tanapat Palaga, Ph.D.)

--Examiner

(Prompong Pienpinijtham, Ph.D.)

--Examiner

(Ratthapol Rangkupan, Ph.D.)

--External Examiner

(Assistant Professor Thitinan Karpkird, Ph.D.)

ฐาปกรณ์ ตรีอุดม : อนุภาคนาโนอัพคอนเวอร์ติง : การสังเคราะห์ พิสูจน์เอกลักษณ์ และ การประยุกต์ใช้ทางชีวเวช (UPCONVERTING NANOPARTICLES: SYNTHESIS, CHARACTERIZATION AND BIOMEDICAL APPLICATION) อ.ที่ปรึกษาวิทยานิพนธ์หลัก: รศ. ดร. ศุภศร วนิชเวชารุ่งเรือง, อ.ที่ปรึกษาวิทยานิพนธ์ร่วม: ดร. นำพล อินสิน, 74 หน้า.

อนุภาคอัพคอนเวอร์ติงคืออนุภาคที่มีความสามารถในการเปลี่ยนโฟตอนพลังงานต่ำให้เป็นโฟตอนพลังงานสูง สมบัติเฉพาะตัวนี้ทำให้อนุภาคอัพคอนเวอร์ติงเหมาะสมสำหรับการประยุกต์ใช้ทางชีวเวช ตัวอย่างเช่น ภาพเรืองแสงของเซลล์ ตัวนำส่งยา และการรักษาแบบโฟโตไดนามิค อย่างไรก็ตามอิทธิพลด้านรูปร่างของอนุภาคอัพคอนเวอร์ติงต่ออันตรกิริยาระหว่างอนุภาคและเซลล์ยังไม่ชัดเจน เพื่อความเข้าใจที่ดีขึ้นในเรื่องนี้ ในที่นี้เราจึงได้เตรียมอนุภาคอัพคอนเวอร์ติงที่เกิดจาก $NaYF_4$ โดปด้วยธาตุ Yb และTm ซึ่งมีรูปทรงที่แตกต่างกันได้แก่ กลม แท่ง และปริซึมขึ้นอนุภาคอัพคอนเวอร์ติงทั้งสามรูปทรงที่กระจายตัวได้ในน้ำมีโครงร่างผลึกและประจุที่พื้นผิวเหมือนกัน ดังนั้นอนุภาคที่เตรียมได้นี้สามารถนำไปศึกษาอันตรกิริยากับลิปิดไบเลเยอร์เมมเบรน การเข้าสู่เซลล์ และความเป็นพิษต่อเซลล์ ผลการทดลองแสดงให้เห็นว่าอนุภาคอัพคอนเวอร์ติงรูปทรงแท่งให้ผลการเข้าสู่เซลล์มะเร็งผิวหนังเมลาโนมา (A-375) และเซลล์มะเร็งตับ (HepG2) สูงที่สุด และมีความเป็นพิษสูงที่สุดเมื่อทดลองกับเซลล์มะเร็งผิวหนังเมลาโนมา (A-375) เซลล์มะเร็งตับ (HepG2) และเซลล์ปอด (WI-38) ผลการทดลองนี้สอดคล้องกับการที่อนุภาครูปทรงนี้เกิดการยึดเหนี่ยวกับลิปิดไบเลเยอร์เมมเบรนดีที่สุดด้วย เนื่องจากอนุภาคอัพคอนเวอร์ติงสามารถเปลี่ยนแสงในช่วงอินฟราเรดย่านใกล้ให้กลายเป็นแสงในช่วงยูวี-วิซิเบิลได้ ในการศึกษานี้คณะผู้วิจัยจึงทำการพัฒนาอนุภาคอัพคอนเวอร์ติงให้มีการเปล่งแสงมากขึ้น จากนั้นบรรจุด้วยสารโฟโตเซนทิไซเซอร์คือ *meso*-Tetraphenyltetrabenzo porphyrinatozinc (ZnTPTBP) อนุภาคอัพคอนเวอร์ติงที่บรรจุด้วยสาร ZnTPTBP แสดงความเป็นพิษต่ำเมื่อทดลองกับเซลล์มะเร็งผิวหนังเมลาโนมา (A-375) และแสดงความสามารถในการทำให้เกิดซิงเกิลทออกซิเจนเมื่อฉายแสงเลเซอร์ที่ความยาวคลื่น 980 นาโนเมตร ที่สำคัญคณะผู้วิจัยแสดงให้เห็นความสามารถของอนุภาคอัพคอนเวอร์ติงที่บรรจุด้วย ZnTPTBP ในการกำจัดเชื้อสิว *Propionibacterium acnes* (*P. acnes*) ภายใต้การฉายด้วยแสงอินฟราเรดย่านใกล้

สาขาวิชา	วิทยาศาสตร์นาโนและเทคโนโลยี	ลายมือชื่อนิสิต	....
ปีการศึกษา	2558	ลายมือชื่อ อ.ที่ปรึกษาหลัก	....
		ลายมือชื่อ อ.ที่ปรึกษาร่วม	....

5487840020 : MAJOR NANOSCIENCE AND TECHNOLOGY

KEYWORDS: UPCONVERTING NANOPARTICLES / NEAR INFRARED LIGHT / SHAPE / LIPID BILAYER MEMBRANE / CELLULAR ASSOCIATION / PHOTODYNAMIC THERAPY / SINGLET OXYGEN / PROPIONIBACTERIUM ACNES

THAPAKORN TREE-UDOM: UPCONVERTING NANOPARTICLES: SYNTHESIS, CHARACTERIZATION AND BIOMEDICAL APPLICATION. ADVISOR: ASSOC. PROF. SUPASON WANICHWECHARUNGRUANG, Ph.D., CO-ADVISOR: NUMPON INSIN, Ph.D., 74 pp.

Upconverting nanoparticles (UCNPs) are particles that possess ability to convert low energy photons into high energy photons. This unique property makes the UCNPs suitable for biomedical applications such as cell fluorescence imaging, drug carriers and photodynamic therapy. However, the influence of the UCNPs morphology toward the particle-cell association is still unclear. Here the UCNPs based on $NaYF_4$ doped with Yb and Tm of different shapes such as sphere, rod and prism are prepared. The three shaped water dispersible UCNPs particles have the same crystal phase structure and surface charge. Therefore, the as-prepared particles can be used for studying lipid bilayer membrane interaction, cellular uptake and cytotoxicity. The results indicate that the rod-shaped UCNPs give the highest cellular uptake into malignant melanoma (A-375) and liver carcinoma (HepG2) cell lines and highest cytotoxicity in A-375, HepG2 and normal lung (WI-38) cell lines. These results correspond well with the result of the highest particle-membrane association observed for this particle shape. Since the UCNPs can upconvert near infrared (NIR) light into lights in the UV-visible region, here we also develop the UCNPs with a highly-upconverted emission and then load the obtained material with a photosensitizer, *meso*-Tetraphenyltetrabenzo porphyrinatozinc (ZnTPTBP). The ZnTPTBP-loaded UCNPs show low toxicity against malignant melanoma (A-375) cell line and possess an ability to generate singlet oxygen when being irradiated with a 980 nm NIR laser. More importantly, we demonstrate the capability of the ZnTPTBP-loaded UCNPs to eradicate *Propionibacterium acnes* (*P. acnes*) under NIR irradiation.

Field of Study: Nanoscience and Technology

Academic Year: 2015

Student's Signature ....

Advisor's Signature ....

Co-Advisor's Signature ....

ACKNOWLEDGEMENTS

CONTENTS

LIST OF TABLES

LIST OF FIGURES

LIST OF ABBREVIATIONS

%	Percent
°C	Degree Celsius
W	Watt
J	Joule
mL	Milliliter
g	Gram
mg	Milligram
μg	Microgram
μl	Microliter
cm	Centimeter
nm	Nanometer
ppm	Parts per million
mM	Millimolar
rpm	Revolutions per minute
rcf	Relative centrifugal force
min	Minute
h	Hour
cm^{-1}	Wavenumber
v/v	Volume by volume

w/w	Weight by weight
w/v	Weight by volume
psi	Pounds per square inch
Da	Dalton
MW	Molecular weight
OD	Optical density
U	Unit
λ	Wavelength
^{1}H NMR	Proton nuclear magnetic resonance
^{13}C NMR	Carbon-13 nuclear magnetic resonance
δ	Chemical shift
d	Doublet
dd	Doublet of doublet
t	Triplet
J	Coupling constant
m/z	Mass to charge ratio

CHAPTER 1

Introduction

1.1 Background

A substance that emits light when it is exposed to light is named as luminescence material. A process in which the luminescent materials emit light upon light excitation is known as photoluminescence. In general, the photoluminescence process can be divided into two groups: (1) down-conversion and (2) up-conversion. Down-conversion is a photoluminescence process commonly occurred in nature. This process emits low energy light after the material is being excited by high energy light. In contrast, up-conversion is the opposite process of down-conversion in which high energy light is emitted when the material is excited with low energy light. This particular process is rarely occurred in nature.[1]

Since the early 1980s, developments in nanoscience and technology have bloomed. The increasing research interests in the field of nanomaterials, particularly, nanoparticles have greatly attracted many researchers. Nanoparticles are normally defined as particles having diameter in a range of 1-100 nanometers (nm). A Nanometer is one billionth of a meter denoted a factor of 10^{-9} meter.

In the further section of this chapter, upconverting nanoparticles (UCNPs) with their properties and applications will be explained in detail.

1.2 Upconversion materials

1.2.1 Upconversion process

Upconverting nanoparticles (UCNPs) have been proposed to be a new generation of luminescence material.[2, 3] The UCNPs are able to absorb the low energy photons, usually near-infrared light (NIR), and convert it into higher energy photons in the UV to the NIR regions.[2, 4-6] The basic structure of the UCNPs consists

of lanthanide (4f) dopant ions embedded in the lattice of inorganic crystal host. The upconversion luminescence process is as follows: electron in the dopant ion with multiple electronic energy levels absorbs photon and transits from the ground state to an intermediate excited state, and this electron in the intermediate state then absorbs another photon and transits further to an excited state. After that this electron in the excited state emits a photon with high energy in order to transit back to the ground state (Figure 1.1).
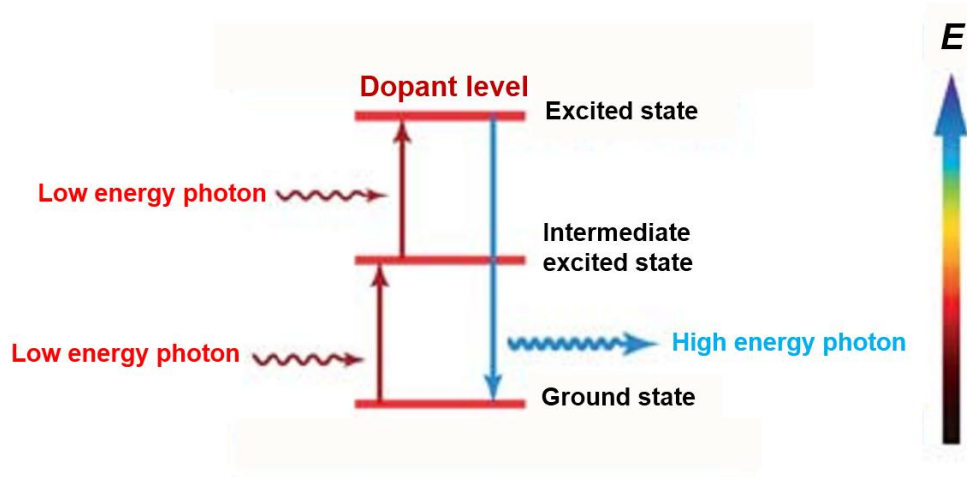
Figure 1.1 Energy level diagram of upconversion luminescence process.

1.2.2 Dopant and host materials

Lanthanide elements, element with an atomic number ranging from 57 (Lanthanum) to 71 (Lutetium), are popularly used as dopant ion in the UCNP. This is owing to their unique electronic configurations and energy level structures. Most of lanthanide elements have ladder-like energy levels of 4f states that allow for sequential multiple photons absorption to take place. The requirement is that the host cations (usually Na^+, Ca^{2+} and Y^{3+} ions) and the dopant ions should have similar radii in order to reduce lattice stain. Low phonon energy of the host material or low chemical bond vibration energy can minimize the non-radiative loss of dopant ions

and thus maximize the efficiency of radiation. It is well known that the upconversion efficiency can be affected by the host materials while upconversion emission wavelength of the dopant lanthanide ions remains unchanged.

1.3 Synthesis methods of upconverting nanoparticles (UCNPs)

Ideal UCNPs should be small in size with narrow size distribution and uniform shape. Thus, a variety of methods to synthesize the UCNPs have been developed. The following sections summarize these methods.

1.3.1 Co-precipitation method

In a typical procedure, a solution of lanthanide chlorides or nitrates is injected into a solution of the host material such as sodium fluoride to form nanoparticles (e.g. $NaYF_4$) that spontaneously precipitate.[1] This method is simple, convenient and allows the UCNPs in controllable size with narrow size distribution, but post heat treatment at high temperature is required in order to acquire the UCNPs with high upconversion efficiency.

1.3.2 Hydro(solvo)thermal method

In a typical procedure, the rare earth precursors and fluoride precursors are mixed together in an aqueous solution, placed in an autoclave and then sealing and heating them. This method uses a solvent under pressures and reaction temperatures over the critical point to enhance the solubility of solids and to accelerate reactions between solid states.[7] The need of special reaction vessels (e.g. autoclave) and the difficulty of reaction monitoring are disadvantages of the method.

1.3.3 Thermal decomposition method

Thermal decomposition is another method to yield the UCNPs with high quality and monodispersed size. In a typical procedure, the rare earth trifluoroacetate precursors are thermally decomposed in the presence of oleic acid and octadecene

to obtain the metal fluorides. The octadecene is used as a solvent due to its high boiling point (b.p. 315 $^{\circ}$C), and the oleic acid not only acts as a solvent but also as a ligand to prevent the particle agglomeration.[8]

Under different synthesis conditions described above, the UCNPs have been obtained with different crystal structures such as hexagonal and cubic phases, and also different morphologies including spheres, tubes, wires, disks, plates, zigzagged rods and flower-patterned disk arrays.[9, 10]

1.4 Optimization of the UCNPs luminescence efficiency

For application of the UCNPs, the upconversion luminescence efficiency is important because high efficiency leads to increased emission intensity. Examples of strategies reported include:

1.4.1 Dopants-host matching

Although a single lanthanide dopant ion is enough to generate the upconversion effect, it still shows the weak emission due to the low absorption cross-section of lanthanide ions. To increase the upconversion efficiency, co-doping between two different lanthanide ions is frequently preferred. One dopant ion acts as an emitter whereas another acts as an absorber. Trivalent lanthanides such as erbium (Er^{3+}) and thulium (Tm^{3+}) ions are commonly used as emitter ion due to their ladder-like energy levels that promote photon absorption and energy transfer in upconversion processes. Conversely, ytterbium (Yb^{3+}) ion is widely used as the absorber ion due to its larger absorption cross-section in the NIR region (around 980 nm) than other lanthanide ions.[2] Another important composition of the UCNPs is the host materials, which define the optical properties and emission efficiency. The suitable host materials should have close lattice matching with the dopant ions and low lattice phonon energies to minimize energy losses and maximize radiative emissions. Nowadays, host materials have been extremely focused on fluoride and oxide nanoparticles such as

NaYF$_4$,[11] LaF$_3$,[12] Y$_2$O$_3$[13] and Gd$_2$O$_3$.[14] Among the available types of the UCNPs, NaYF$_4$ co-doped with Yb^{3+}, Er^{3+} or Yb^{3+}, Tm^{3+} nanoparticles have been reported as the materials with the highest upconversion efficiency.[15] Under a 980 nm NIR excitation, Yb^{3+}, Er^{3+} co-doped the UCNPs exhibit green emissions at 525 and 550 nm which correspond to the transitions from the ^{2}H$_{11/2}$ and ^{4}S$_{3/2}$ excited states to the ^{4}I$_{15/2}$ ground state and red emission at 660 nm from the ^{4}F$_{9/2}$ excited state to the ground state ^{4}I$_{15/2}$ (Figure 1.2).[16] For Yb^{3+}, Tm^{3+} co-doped the UCNPs, the emission bands at 451, 481, 646 and 800 nm have been assigned to ^{1}D$_2 \longrightarrow$ ^{3}F$_4$, ^{1}G$_4 \longrightarrow$ ^{3}H$_6$, ^{1}G$_4 \longrightarrow$ ^{3}F$_4$ and ^{3}H$_4 \longrightarrow$ ^{3}H$_6$ transitions, respectively. In addition, the emission at 365 nm assigned to ^{1}D$_2 \longrightarrow$ ^{3}H$_6$ can also be detected (Figure 1.2).[16]
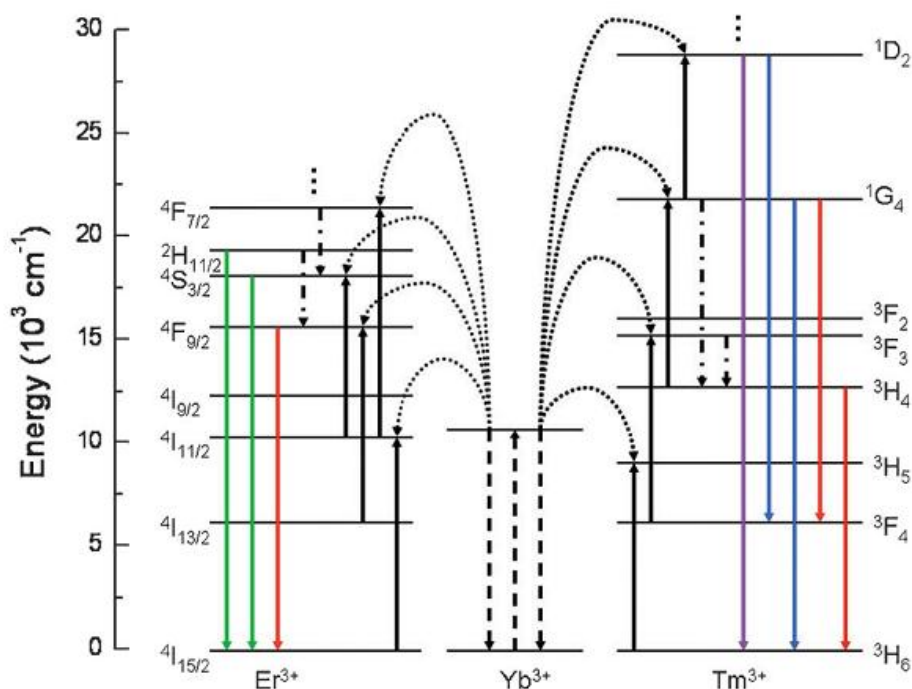
Figure 1.2 Proposed energy transfer mechanisms of Er^{3+}, Tm^{3+} and Yb^{3+} co-doped UCNPs under 980 nm excitation.[16]

1.4.2 Formation of hexagonal phase

The crystal structures of $NaYF_4$ host exhibit two phases, (α) cubic and (β) hexagonal phase, which is depending on the synthesize condition. There is a report showed that the upconversion efficiency of the green emission in the hexagonal-phase $NaYF_4$:Yb^{3+}, Er^{3+} UCNPs is approximately 10 times stronger than that in cubic phase.[11, 17] Therefore, control of the $NaYF_4$ crystal structure to form a pure hexagonal phase is extremely important for high upconversion luminescence efficiency.

1.4.3 Doping concentration

Doping concentration is one of the significant parameters for upconversion process. Basically, the upconversion emission intensity can be enhanced by increasing the concentration of lanthanide dopants in the material but there is a critical concentration in which above this point, emission intensity is severely quenched by cross-relaxation mechanism.[18] The upper limit of concentration usually depends on an exact distance of lanthanide ions in host lattice.[17] Therefore, the optimal concentration of dopants need to be considered.

1.4.4 Preparation core/shell structure

Another strategy to increase the luminescence efficiency of the UCNPs is the construction of core/shell architecture where a shell of material is grown around the UCNPs to reduce non-radiative decay losses from the surface material. Studies of the core/shell $NaYF_4$:Yb^{3+}, Er^{3+} (Tm^{3+})/$NaYF_4$ nanoparticles have been reported to enhance the upconversion luminescence intensity comparing with the uncoated nanoparticles.[19-22]

1.5 Surface modification strategies of UCNPs

The UCNPs used for biomedical applications should be water dispersible and provide active functional groups. A surface functionalization is required for changing hydrophobic UCNPs into hydrophilic ones and allows further reaction with biomolecules. To date, the surface functionalization can be accomplished through ligand exchange, ligand oxidation, ligand attraction, layer by layer assembly, silanization and also host-guest interaction strategies. The following sections summarize these strategies.

1.5.1 Ligand exchange

This strategy involves the replacement of native hydrophobic ligands on the upconverting nanoparticles surface by bifunctional molecules. Boyer and coworkers [23] have demonstrated ligand exchange of oleic acid ($CH_3(CH_2)_7CH=CH(CH_2)_7COOH$) with PEG-phosphate ($CH_3OCH_2(CH_2OCH_2)_nCH_2OPO_3$) for the fabrication of water soluble $NaYF_4$: Yb, Er nanoparticles. The carboxyl groups of oleic acid ligand were replaced by phosphate groups of poly(ethylene glycol) phosphate to obtain water soluble nanoparticles.

1.5.2 Ligand oxidation

This strategy involves oxidation reaction of the native ligands containing carbon-carbon double bond (C=C) with Lemieux-von Rudloff reagent. To provide water soluble upconverting nanoparticles with dual carboxylic acid functionalized surface, Chen and coworkers [24] have presented the conversion of oleic acid ligand ($CH_3(CH_2)_7CH=CH(CH_2)_7COOH$)-capped $NaYF_4$: Yb, Er/Ho/Tm to azelaic acids ($HOOC(CH_2)_7COOH$) using the Lemieux-von Rudloff reagent.

1.5.3 Ligand attraction

This strategy involves the assembly of an amphiphilic copolymer onto the particle's surface through the hydrophobic van der Waals interaction between native ligand and the hydrocarbon chain of the polymer. Cheng and coworkers [25] have demonstrated the coating of octylamine-poly(acrylic acid)-poly(ethylene glycol) amphiphilic copolymer onto the $NaYF_4$:Yb, Er/Tm nanoparticles. The water soluble upconverting nanoparticles were formed by hydrophobic interactions between hydrocarbon chains of the octylamine and the native oleic acid ligand.

1.5.4 Layer by layer assembly

Layer by layer assembly involves the electrostatic adsorption between oppositely charged polyions. Wang and coworkers [26] have developed a layer by layer method to transfer hydrophobic $Na(Y_{1.5}Na_{0.5})F_6$:Yb^{3+}, Er^{3+} nanoparticles into water soluble form, based on the layer by layer deposition of positively charged poly(allylamine hydrochloride) and negatively charged poly(styrene sulfonate).

1.5.5 Silanization

The basic concept involves the growing of a silica layer on the particles surface through the hydrolysis and polycondensation reaction of siloxane monomers. Sivakumar and coworkers [27] have performed the utilization of silica for coating the LaF_3: Yb, Er/Tm nanoparticles. The silica layer was formed by hydrolysis and polycondensation of tetraethyl orthosilicate (TEOS), which was used as a precursor. The silica coated nanoparticles have a uniform size distribution and can be dispersed in aqueous solution.

1.5.6 Host-guest interaction

Host-guest interaction involves the hydrophobic interaction of host molecule cyclodextrin which contains glucopyranose group and a hydrophobic cavity, and the

guest hydrophobic molecule. Liu and coworkers [28] have reported a host-guest self-assembly technique that uses the interaction between alpha cyclodextrin (α-CD) as a host molecule and oleic acid ligand as a guest molecule to make $NaYF_4$: Yb, Er/Tm nanoparticles soluble in water.

1.6 Biomedical-applications of UCNPs

Comparing with conventional luminescence probe such as organic dye and quantum dot, UCNPs are promising as a new luminescence probe. This is because UCNPs possess ability to be excited by NIR light whereas the conventional luminescence materials usually were excited by UV or visible light. Due to the intrinsic upconversion luminescence properties of the UCNPs, they directly provide many advantages. Excitation with NIR can minimize photodamage to biological samples.[3] This is due to weak absorption of biological matter. NIR light maximizes tissue penetration.[29] UV light can penetrate into the skin only 1-2 mm whereas NIR light penetration is at least 1 cm. Lastly, with emission in the visible region and excitation in the NIR, auto-fluorescence background from the tissue samples cannot interferes the fluorescence signal.[30] This is due to optical transparency of any biological tissue in infrared region. Moreover, the UCNPs exhibit high photostability and less photobleaching for long period of observation, comparing with conventional fluorophores [31], thus making the UCNPs suitable to utilize in biomedical field. In recent years, many reports have demonstrated the utilization of UCNPs on photoluminescence imaging of cell and tissue [32-34], drug delivery [34-37] and cancer treatment with their luminescence such a photodynamic therapy.[38-42]

The detail of each applications will be discussed in following sections.

1.6.1 Cell imaging

Cell imaging is an effective tool to understand the fundamental nature of cell and function of tissue. Since the development of UCNPs, the materials have been

widely used as contrast stains for *in vitro* and *in vivo* imaging applications. In addition, these nanoparticles have been employed for broad purposes ranging from general to specific detections of targeted molecules. To image of specific target structures, the conjugation of UCNPs with recognition molecules such as antigen-antibody and ligand-acceptor have been demonstrated.

The first report on cell and tissue imaging using polyethyleneimine (PEI) coated $NaYF_4$:Yb,Er nanoparticles with spherical shape and diameter of 50 nm was published in 2008 by Chatterjee and coworkers.[43] Later, further studies indicated that UCNPs incubated with cell lines can be endocytosed by cells and shown strong luminescence signal without autofluorescence upon NIR irradiation.[23, 44-46] Interestingly, imaging of cells based on UCNPs with no fading effect even after hours of NIR irradiation have been reported by Yu and coworkers.[31] Targeted imaging of cells have also been studied by using UCNPs modified with specific biomolecules. For example, antibody conjugated $NaYF_4$:Yb, Er nanoparticles can be specifically bind to antigen express on cell membrane for highly immunolabeling and imaging of cancer cell *in vitro*.[30]

Recently, the photoluminescence imaging based on UCNPs has been extended for *in vivo* imaging of small animals. Chatterjee and coworkers [43] have demonstrated that PEI coated $NaYF_4$: Yb, Er nanoparticles can be used for imaging of deep tissues in rats. The upconverting nanoparticles showed visible fluorescence up to 10 mm in depth beneath the skin when exposed to a near infrared laser at 980 nm whereas quantum dots injected into abdomen under ultraviolet excitation gave no observable fluorescent signal

Although many publications have been successfully demonstrated the application of UCNPs for bioimaging, a challenge is to develop UCNPs with higher emission efficiency. This is because brightness is one of the critical issues for UCNPs to be used in commercial applications.

1.6.2 Photodynamic therapy

Photodynamic therapy (PDT) is well known as a clinical acceptance and a minimally invasive treatment for several diseases including cancer. PDT basically composes of three main factors (1) a light source (2) a photosensitizer and (3) oxygen. Light in PDT is used for activation of photosensitizer molecule from a ground state into an excited state. The mechanism of PDT is based on the interaction between the excited photosensitizer and oxygen molecules for generating reactive oxygen species (ROS) such as singlet oxygen, leading to oxidative damage of biological matters and cell death. Since PDT light confines the damage only the target areas therefore PDT provides many advantages including localized killing area and minimized side effects. However, most photosensitizers are excited by visible light which limits the treatment in deep tissues. To avoid this limitation, NIR light that provides higher penetration depths can be used in place of visible light; however, the approach to convert NIR light into visible light is required.

To fulfill that requirement, using UCNPs is suggested as one approach. Under excitation by NIR light, the upconverted visible emission from these nanoparticles can be absorbed by photosensitizers, and then energy from the excited photosensitizer is transferred to oxygen molecules to generate reactive oxygen species (ROS) for killing effect. Therefore, apart from imaging, UCNPs have been reported for serving as delivery vehicles in drug delivery and acting as nanotransducers in photodynamic therapy.

The application of UCNPs based PDT in cancer cell was firstly reported by Zhang and coworkers in 2007.[47] The photosensitizer coated UCNPs were incubated with cancer cells. Under NIR irradiation, cell death was observed within one hour of incubation. To improve the therapeutic efficiency, high loading photosensitizer on UCNPs were successfully prepared by Ungun and coworkers.[48] The particles: photosensitizer ratio was increased up to 3:1. Under NIR irradiation, singlet oxygen

generation was also detectable by monitoring the decrease of fluorescence intensity of 9,10-anthracenedipropionic acid. Another interesting was demonstrated by Qian and coworkers,[49] the photosensitizer was designed to impregnate into a mesoporous silica shell on UCNPs in order to improve the release of singlet oxygen. The efficiency of this design on therapeutic action was exhibited in the fluorescence quenching of 9,10-anthracencediyl-bis(methylene)dimalonic acid and reduction of cell viability of cancer cells.

1.7 Objectives

In recent years, UCNPs have been prepared for use as near-infrared imaging agents, therapeutic agents and drug carriers. The lack of information on the influence of particle morphology toward the particle-cell association makes it difficult to select the appropriate shape for each application. In addition, most of works on the application of UCNPs in PDT have been mainly focused on cancer treatment while the bacterial infection disease treated by PDT is very interesting and needed to be investigated. Therefore, the objectives of this study include:

I. Investigation on the UCNPs shape effect on cellular interaction

1. Synthesis of UCNPs base on $NaYF_4$ co-doped with Yb^{3+} and Tm^{3+} of three different shapes i.e. nanosphere, nanorod and nanoprism using thermal decomposition method.

2. Surface modification of three shaped UCNPs by poly(ethylene glycol)diacid ligand using ligand exchange strategy to produce water-dispersible UCNPs and further covalent linking the ligand with fluorescent molecule.

3. Study of the shape effect of the modified UCNPs on cell cytotoxicity, cellular uptake and artificial lipid bilayer membrane association using the prepared fluorescently labelled UCNPs.

II. Finding UCNPs with maximum UV visible emission

4. Study the effect of Tm^{3+} concentration on $NaYF_4:Yb^{3+}$, Tm^{3+} core structure UCNPs toward their emission property.

5. Construction of undoped $NaYF_4$ shell on UCNPs core for emission intensity enhancement.

III. Investigation on the antibacterial PDT application of the obtained UCNPs

6. Use core/shell structure UCNPs to further load with photosensitizer, *meso*-tetraphenyltetrabenzo porphyrinatozinc (ZnTPTBP), and study their emission property.

7. Study of cell cytotoxicity and singlet oxygen production of ZnTPTBP-loaded UCNPs under irradiation by a 980 nm NIR laser.

8. Demonstration of photodynamic therapy for *in vitro* photoinactivation of *Propionibacterium acnes* (*P. acnes*) using ZnTPTBP loaded UCNPs together with NIR light.

1.8 Outline of the thesis

The outline of this thesis is presented as following:

1. Synthesis, characterization and surface modification of different shaped UCNPs (Chapter 3).

2. Cytotoxicity, cellular uptake and cell-sized liposome association of the three different shaped UCNPs (Chapter 4).

3. Synthesis, characterization and surface modification of core/shell-UCNPs and their upconversion emission properties (Chapter 5).

4. Photosensitizer-loaded core/shell-UCNPs and their application in antimicrobial photodynamic therapy (Chapter 6).

CHAPTER 2

Characterization techniques

2.1 X-ray powder diffraction (XRD)

XRD is a non-destructive analytical tool primarily used for identification of crystal structure and chemical composition of material. When monochromatic X-rays are directly hit onto a sample, crystalline atoms cause a beam to diffract into specific directions. Then, the diffraction intensity of the X-ray beam is collected as a function of the incident and angle. In this thesis, XRD patterns were obtained using a DMAX 2200/Ultima+ diffractometer (Rigaku, Tokyo, Japan) using Cu Kα radiation source and operating at 40 kV and 30 mA. The XRD spectra were collected with a scan range of 10°- 80° and scan speed of 1°/min.

2.2 Transmission electron microscopy (TEM)

TEM is a powerful microscopic technique for material observation in nanoscopic scale. TEM requires an electron beam with high energy to pass through a sample. Since electrons have smaller de Broglie wavelength, therefore they are able to interact with sample in atomic level. The interaction between the transmitted electrons and the atoms of sample can be used to generate the image. The contrast of TEM image is owing to the absorption of electrons, thus is related to thickness and composition of the material. In this thesis, TEM images were obtained using a TECNAI 20 TWIN transmission electron microscope (FEI Company, OR, USA) operating at 120 kV. The dilute dispersion of oleate capped UCNPs in hexanes or PEG-coated UCNPs in milliQ water was dropped on carbon film on 200 mesh copper grids and then dried in desiccators at room temperature. The average size of the UCNPs was measured from several TEM images of UCNPs using SemAfore program.

2.3 Zeta potential

Zeta potential is a measurement of electrostatic or charge attraction-repulsion between particles. Particles which are dispersed in an aqueous solvent can generate a surface charge through the ionization of surface functional groups or adsorption of charged species. These surface charges make the distribution of the surrounded ions, leading to formation of a double layer around the particle. Zeta potential value is determined as electrical potential in the double layer at a slipping plane (Figure 2.1). This value provides details in the causes of dispersion or aggregation which can be indicated a stability of colloidal particles. It means that colloidal dispersions with high zeta potential (negative or positive) are stable whereas colloid dispersions with low zeta potential are likely to aggregate. In this thesis, the measurement of zeta potential of UCNPs in milliQ water was performed using a Malvern Zetasizer nanoseries model S4700 (Malvern Instruments, Worcestershire, UK) using a He–Ne laser beam at 632.8 nm and scattering angle of 173°.
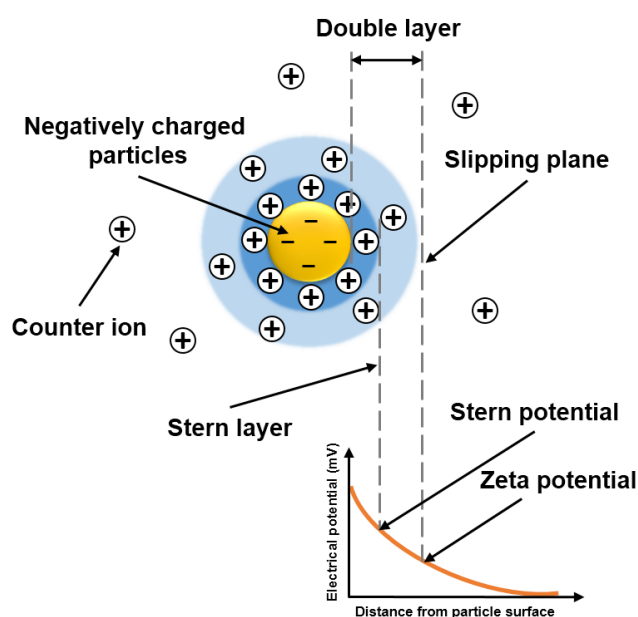
Figure 2.1 Potential difference as a function of distance from particle surface.

2.4 Attenuated total reflectance fourier transform infrared spectroscopy
(ATR-FTIR)

FTIR spectroscopy is a technique that provide an infrared spectrum of absorption, emission or transmission of a solid, liquid or gas. Infrared transmission spectrum obtained from this technique is very useful for determination of chemical bonds in a molecule. The vibration of different chemical bonds can be identified through the infrared light absorption at specific wavelengths. In this thesis, IR spectra were acquired from a Nicolet 6700 (Thermo Scientific, MA, USA) coupled with a diamond ATR crystal. The spectra were recorded at resolution of 2 cm^{-1} and 64 numbers of scans.

2.5 Ultraviolet-Visible absorption spectroscopy (UV-Vis)

UV-Vis spectroscopy is related to absorption spectroscopy in the UV and visible region. This technique is commonly used for quantitative measurement of analytes, such as conjugated organic compounds, transition metal ions, and biological molecules. UV-Vis spectroscopy is complementary to fluorescence spectroscopy in which the fluorescence technique measures transitions of electrons from the excited state to the ground state, whereas absorption spectroscopy measures transitions of electrons from the ground state to the excited state. The energy gap between the ground state and excited state can be observed through the absorption wavelengths, and this information is directly related to the electronic energy level of the molecules and thus is related to the molecular structure of the analyte. In this thesis, absorption analysis were carried out in dispersions in 1 cm quart cuvette using an Optizen Pop QX UV–Vis spectrophotometer (Mecasys, South Korea).

2.6 Fluorescence spectroscopy

This analytical technique detects fluorescence signal emitted from molecules usually with ultraviolet or visible light as an excitation source. Once the molecule is

excited by photon absorption, the electrons in the molecule transit from their ground state to one of the vibrational energy levels in the excited electronic state. Then, the electrons move down vibrational levels within the excited electronic energy level until they reach the ground state vibrational energy level of that excited electronic level, through the non-radiative pathway. Then the elecron move accross the excited elecronic energy level down to the ground state energy level through the radiative pathway, thus emitting photons. The frequencies of emitted light are related to the gap between the electronic energy level within the molecules and therefore can be used to determine the structure of the molecule. In this thesis, emission spectra were collected in 1 cm quart cuvettes by an Agilent cary eclipse fluorescence spectrophotometer (Agilent Technologies, CA, USA).

2.7 Upconversion luminescence spectroscopy

In this thesis, upconverted emission spectra were recorded under an excitation with a 980 nm continuous-wave laser coupled to 1 m optical fiber (Changchun New Industries Optoelectronics Technology, Changchun, China). UCNPs sample was dispersed in hexane or milliQ water and placed in a QS quartz cuvette (path length of 1 cm). The upconverted emissions were detected at 90 ° with respect to the laser excitation beam using a USB2000 fiber optic spectrometer (Ocean Optics, FL, USA) considered as a detector.

2.8 Inductively coupled plasma-optical emission spectroscopy (ICP-OES)

ICP-OES is an analytical technique that used to determine trace of elements. Sample is injected into a radiofrequency-induced argon plasma using nebulizer, quickly dried and vaporized at high temperature. Thus, the elements are available as free atoms and ions in the gas phase. Collisional excitation by plasma can also promote atoms and ions to the excited states and the excited atomic and ionic may then relax to the ground state via a photon emission. This technique is based on the spontaneous

emission of photons from excited atoms and ions. These photons have their own characteristic energies determined by the quantized energy level. Thus, the wavelength of the photons can be used to identify type of the elements in sample and the obtained intensity of this emission can be associated with the concentration of the elements. With this technique, the concentration can be quantitatively analyzed down to ppb level. In this thesis, the Y^{3+}, Yb^{3+} and Tm^{3+} contents in $NaYF_4$: Yb^{3+}, Tm^{3+} samples were analyzed using an iCAP 6500 ICP emission spectrometer (Thermo Scientific, MA, USA). Five milligrams of as-synthesized sample was digested in concentrated nitric acid at 80 °C for 20 h and diluted with milliQ water before analysis. Calibration was performed by analyzing serial dilutions of standard elements.

2.9 Confocal laser fluorescence scanning microscopy (CLFM)

CLFM is an effective microscope for observation of high-resolution optical imaging at selected depth. In CLFM, lasers are used as a light source to excite fluorophores in a specimen. Image details are gathered point by point using a detector such as photomultiplier tube or photodiode, and then digitized for processing by computer. Because this technique has an ability to control the depth of interested field, the image details from other depths in the specimen are not superimposed. Moreover, CLFM offers the ability to reduce background away from the focal plane and the capability to collect the optical sections from thick specimen. Thus, quality of the image is obviously enhanced over simple microscope. For biological application, the specimen is often labeled with fluorescence dye to make the desired objects visible. In this thesis, cell imaging was performed using an Eclipse-C1 Ti series confocal laser scanning fluorescence microscope (Nikon, Tokyo, Japan) with an excitation wavelength of 488 nm and detection at 525 nm.

2.10 Flow cytometry

Flow cytometer is an instrument used for cell counting, cell sorting, protein engineering and biomarker detection. To use this technique, fluorescence dyes must be bound to cellular components or delivered into cells. The dye-containing cells are suspended in a stream of fluid and passed singly through the laser beam. Thus, fluorescent molecules in the cells are excited to a higher energy level and emit light upon returning to their resting state, thus producing fluorescence signals. The fluorescence signals are detected by photomultiplier and processed into electrical signals by computer. The data acquired by this technique can be plotted in a single dimension to produce a histogram or plotted in two dimensional dot plots format. The region on these plots can be separately seen, depending on the difference of fluorescence intensity. In this thesis, intracellular fluorescence detection was performed on a Cytomics FC500MPL (Becman Coulter Inc., NY, USA) flow cytometer flow using laser at an excitation wavelength of 488 nm and detection at 525 nm. At least 10,000 cells were measured for each sample. The acquired data were analyzed by FlowJo software (Tree Star, Inc.).

CHAPTER 3

Synthesis, characterization and surface modification of different shaped UCNPs

In this chapter, we report the synthesis of different shaped UCNPs. The effect of ligand/solvent ratio on particle shape was studied. To allow the obtained hydrophobic UCNPs to disperse in water, the original ligand was replaced by a hydrophilic one using a ligand exchange strategy. Moreover, different shaped UCNPs with fluorescence labeling were prepared.

3.1 Experimental details

3.1.1 Materials

All chemicals and reagents were used as received. $YCl_3 \cdot 6H_2O$ (99.99%), $YbCl_3 \cdot 6H_2O$ (99.99%), $TmCl_3 \cdot 6H_2O$ (99.99%), oleic acid (90%), 1-octadecene (90%), ammonium fluoride (NH_4F), sodium hydroxide (NaOH) and Poly(ethylene glycol)bis(carboxymethyl)ether (PEG-600-diacid, average M_n = 600) and 6-aminofluorescein (95%, bioreagent) were purchased from Sigma-Aldrich (Steinheim, Germany). 1-(3-Dimethylaminopropyl)-3-ethylcarbodiimide hydrochloride (EDC), N-hydroxysuccinimide (NHS) were purchased from Acros Organics (Geel, Belgium). Ethanol and methanol were purchased from Merck (Darmstadt, Germany).

3.1.2 Synthesis of oleate capped UCNPs (oleate-UCNPs) with different shapes

Oleate-caped upconverting nanosphere (oleate-NS): $YCl_3 \cdot 6H_2O$ (2.78 mmol, 843.3 mg), $YbCl_3 \cdot 6H_2O$ (1.2 mmol, 465 mg) and $TmCl_3 \cdot 6H_2O$ (0.02 mmol, 7.7 mg) were weighted and loaded into a three-neck round-bottom flask containing 24 mL of oleic acid and 60 mL of octadecene. The mixture was magnetically stirred and slowly heated to 130 °C for 40 min under vacuum to form a transparent pale-yellow solution and then cooled down to room temperature. Twenty milliliter of methanol containing

NaOH (10 mmol, 400 mg) and NH_4F (16 mmol, 592.64 mg) was added dropwise into the reaction flask. The transparent solution became turbid and the resulting cloudy mixture was continuously stirred for 40 min. The mixture was then heated at 75 °C until the methanol was completely evaporated. Afterwards, the reaction temperature was rapidly increased to 300 °C for 90 min with continuous stirring under the nitrogen gas flow. The obtained brown-yellowish solution was then cooled down to room temperature, and the particles were precipitated by the addition of anhydrous ethanol. The precipitates were isolated by centrifugation (GL21M Changsha Yingtai instrument, China) at 5000 rpm (2688 rcf) and washed repeatedly with anhydrous ethanol.

Oleate-caped upconverting nanorod (oleate-NR): The synthesis procedure was performed following a similar procedure as describe above but the amount of both oleic acid and octadecene were adjusted to 42 mL.

Oleate-caped upconverting nanoprism (oleate-NP): The synthesis of the oleate-NP was similar to the oleate-NS but the amount of oleic acid and octadecene were adjusted to 12 mL and 72 mL, respectively.

3.1.3 Synthesis of water dispersible UCNPs (COOH-PEG-UCNPs)

The oleate-UCNPs (50 mg) was loaded into a glass vial containing 125 mg of PEG-600-diacid ligand in 5 mL of ethanol. The vial was capped and sonicated for 15 min. The mixture was heated at 75 °C overnight after that the reaction temperature was cooled down to room temperature. In order to precipitate out the particles, hexane was allowed to add drop-wise into the mixture. The obtained particles were isolated by centrifugation at 8000 rpm (6880 rcf) and repeatedly washed with ethanol to remove the unbounded ligand. The PEG coated sphere, rod and prism shaped UCs was named as COOH-PEG-NS, COOH-PEG-NR and COOH-PEG-NP, respectively.

3.1.4 Synthesis of fluorescent labeled UCNPs (f-UCNPs)

EDC (20 mg) was added into a 20 mL aqueous suspension of the COOH-PEG-UCNPs (1 mg/mL) and stirred at 0 ^{O}C under nitrogen atmosphere for15 min. Then, a 25 µL of acetone solution containing NHS (12 mg) and 6-aminofluorescein (0.12 mg) was introduced and the reaction was kept stirring overnight. The obtained products were collected by centrifugation at 8000 rpm (6880 rcf) and repeatedly washed with a mixture of water and acetone until 6-aminofluorescein was not detected from the supernatant. The fluorescein labeled sphere, rod and prism shaped UCNPs were named as f-NS, f-NR and f-NP, respectively. The fluorescein contents on f-NS, f-NR and f-NP were quantitatively verified by fluorescence spectrophotometer with the aid of calibration curve.

3.2 Characterization

3.2.1 Oleic acid capped sphere, rod, prism shaped upconverting nanoparticles (oleate-UCNPs)

In this study, NaYF$_4$-based UCNPs were synthesized using the thermal decomposition method. Oleic acid was used as ligand to control shape and size of UCNPs. Thus, the different shapes were obtained when the amount of oleic acid was changed. Transmission electron microscopy (TEM) was used to observe the particles morphology and their size. The average size was calculated from approximately 100 particles using SemAfore program. TEM photographs of UCNPs showed that when the volume ratio of oleic acid: octadecene was equal to 2:5 (24 mL oleic acid: 60 mL octadecene), the obtained products were spherical in shape (oleate-NS). The particles size was 26.82±0.52 nm (Figure 3.1a). As the ratio of oleic acid: octadecene was increased to 1:1 (42 mL oleic acid: 42 mL octadecene), upconverting nanorods (oleate-NR) with a length of 37.98±0.72 nm and a width of 24.71±0.94 nm were obtained (Figure 3.1b). Hexagonal prism nanocrystals (oleate-NP) were produced using the ratio

of oleic acid: octadecene of 1:6 (12 mL oleic acid: 72 mL octadecene). The nanoprism had a flat hexagonal top surface with an edge length of 47.88±2.73 nm and six rectangular side surfaces with a surface area of 64.21±1.82 nm x 87.56±3.11 nm (Figure 3.1c).
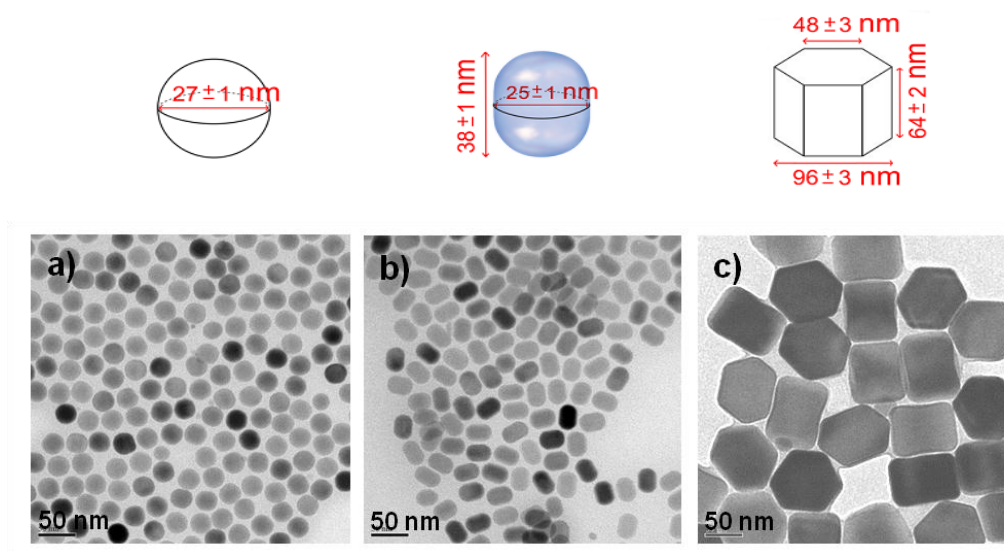
Figure 3.1 Representative TEM photographs of a) oleate-NS, b) oleate-NR and c) oleate-NP. All scale bars indicate 50 nm.

The X-ray diffraction (XRD) was carried out to examine the crystal structure of as-synthesized UCNPs including oleate-NS, oleate-NR and oleate-NP. As shown in Figure 3.2, the peak position of all samples matched well with the diffraction pattern of the standard reference pattern of hexagonal phase-NaYF$_4$ (Joint Committee on Powder Diffraction Standards (JCPDS), file number 28-1192) and no other phases were indexed. This indicated that all three shaped particles were pure hexagonal phase NaYF$_4$ (β-NaYF$_4$). Therefore, there were no adverse effects on the crystal structure of the as-synthesized UCNPs.
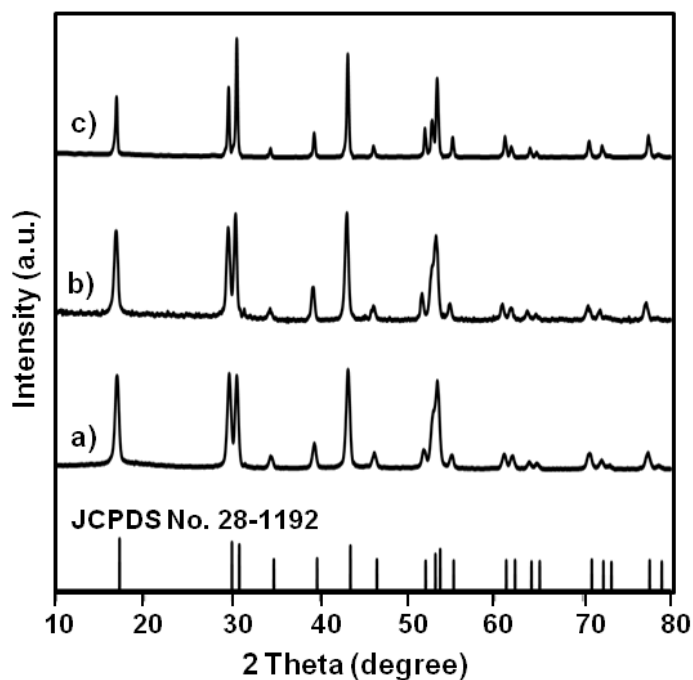
Figure 3.2 XRD patterns of a) oleate-NS, b) oleate-NR and c) oleate-NP in comparison with standard reference β-NaYF$_4$ (JCPDS file number 28-1192).

3.2.2 Water dispersible upconverting nanocrystals (COOH-PEG-UCNPs)

Since the as-synthesized UCNPs were capped by hydrophobic oleic acid molecules, they could be easily dispersed in nonpolar solvents such as chloroform and hexane. This may limit the possibilities for biological applications. To overcome that limitation, the hydrophobic UCNPs were transferred to hydrophilic phase through ligand exchange reaction. The original hydrophobic oleic acid molecules on the UCNPs surface were replaced by PEG-600-diacid (Figure 3.3).

25

Oleate-UCNPs   **COOH-PEG-UCNPs**
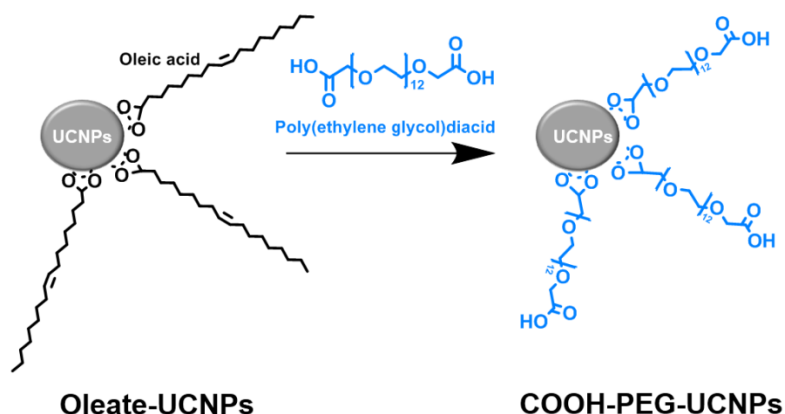
Figure 3.3 Schematic diagram of chemical structure of oletae-UCNPs (before ligand exchange) and COOH-PEG-UCs (after ligand exchange).

Attenuated total reflectance fourier transform infrared (ATR-FTIR) spectroscopy was used to characterize the functional groups present on the surface of oleate-UCNPs and COOH-PEG-UCNPs represented before and after ligand exchange, respectively. Figure 3.4a showed FTIR spectrum of oleate-NR, two peaks at 2921 and 2853 cm^{-1} were assigned to the stretching vibration of C–H whereas the other one around 1710 cm^{-1} is attributed to stretching vibration of C=O. Interestingly, the two peaks appear at 1558 and 1462 cm^{-1} corresponding to asymmetric and symmetric vibration modes of carboxylate forms (COO$^-$), respectively, indicating the adsorption of oleic acid ligands on UCNPs surface. After ligand exchange with PEG-600-diacid, it was found that the characteristic peak of the asymmetric and symmetric stretching vibrations of carboxylate forms (COO$^-$) appeared at 1610 and 1459 cm^{-1}, respectively. Moreover, the stretching mode of the COOH group at 1734 cm^{-1} was also observed, indicating the presence of the free -COOH groups on the particle surface. The new peaks at 1104 cm^{-1} (C-O-C stretching vibration) and 2872 cm^{-1} (C-H stretching vibration) corresponding to characteristic of ethylene glycol supported the presence of PEG (Figure 3.4b)
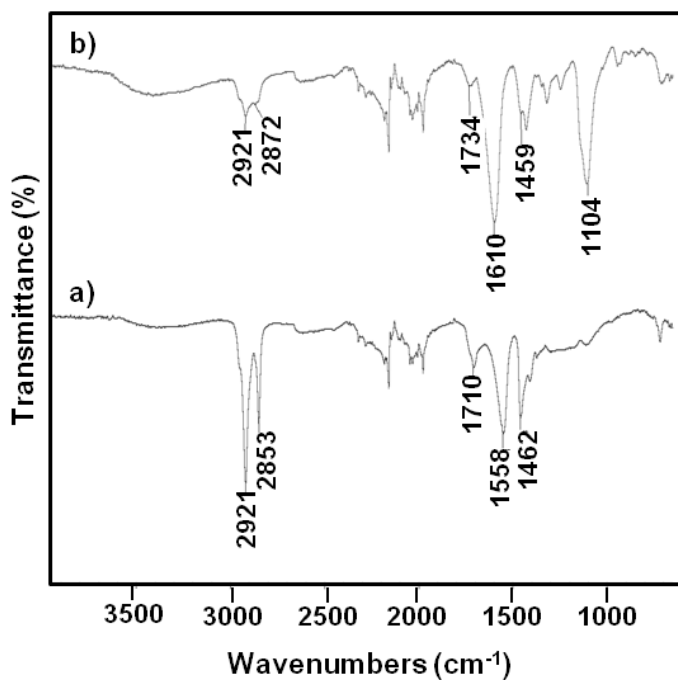
Figure 3.4 ATR-FITR spectra of a) oleate-NR and b) COOH-PEG-NR.

The obtained COOH-PEG-UCNPs also showed good dispersibility in water, suggesting that the hydrophobic oleate had been replaced by hydrophilic PEG-600-diacid. In addition, the zeta potential measurements of the COOH-PEG-UCNPs in milliQ water showed a negative charge (-23.8±0.17 mV for COOH-PEG-NS, -17.7±0.97 mV for COOH-PEG-NR and -9.83±0.18 mV for COOH-PEG-NP). This was due to the presence of negatively charged carboxylate groups (COO^-) on their surface. For morphological observation, TEM photographs confirmed that the COOH-PEG-UCNPs had no obvious changes in shape comparing with the original UCNPs (Figure 3.5).
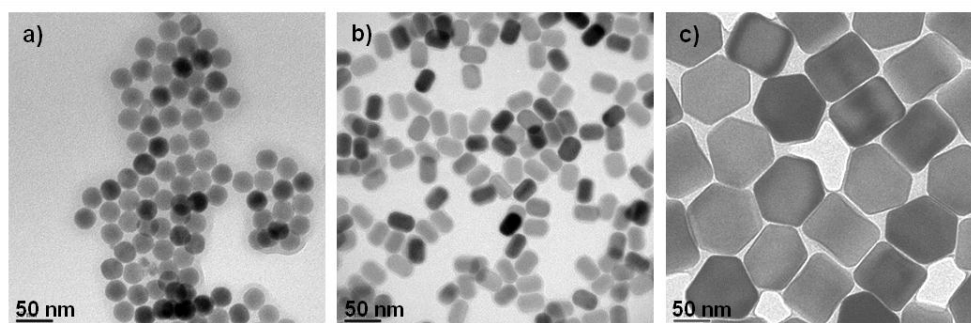
Figure 3.5 Representative TEM photographs of a) COOH-PEG-NS, b) COOH-PEG-NR and c) COOH-PEG-NP. All scale bars indicate 50 nm.

3.2.3 Fluorescent labeled upconverting nanoparticles (f-UCNPs)

The presence of free carboxylic acid groups on COOH-PEG-UCs surfaces not only enhance particle water dispersibility but also allow chemical conjugation. To enable the monitoring of cellular internalization of various shaped particles, a green fluorescent dye, 6-aminofluorescein, was covalently conjugated to carboxylic group of the COOH-PEG-UCNPs by a carbodiimide assisted esterification reaction to obtain f-UCNPs (f-NS, f-NR and f-NP) (Figure 3.6).
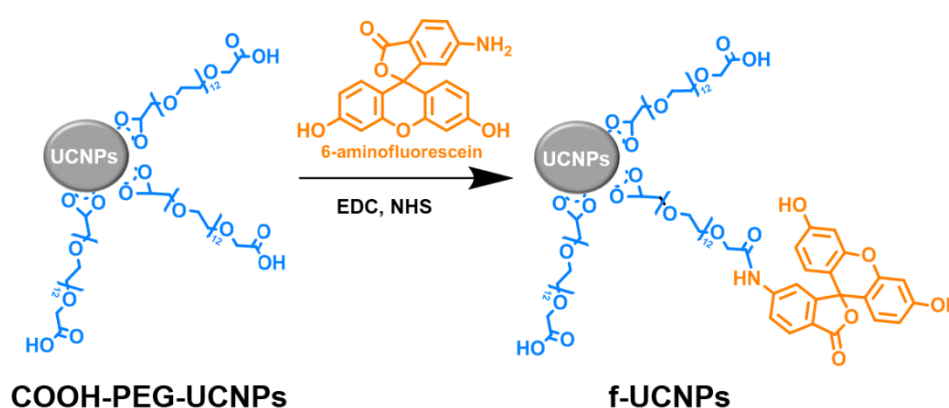
Figure 3.6 Schematic diagram of chemical reaction of f-UCNPs production.

As shown in Figure 3.7, the presence of a new absorption peak at ~ 1640 cm^{-1} (amide I) in the ATR-FTIR spectra of all three samples verified the success of fluorescein grafting.
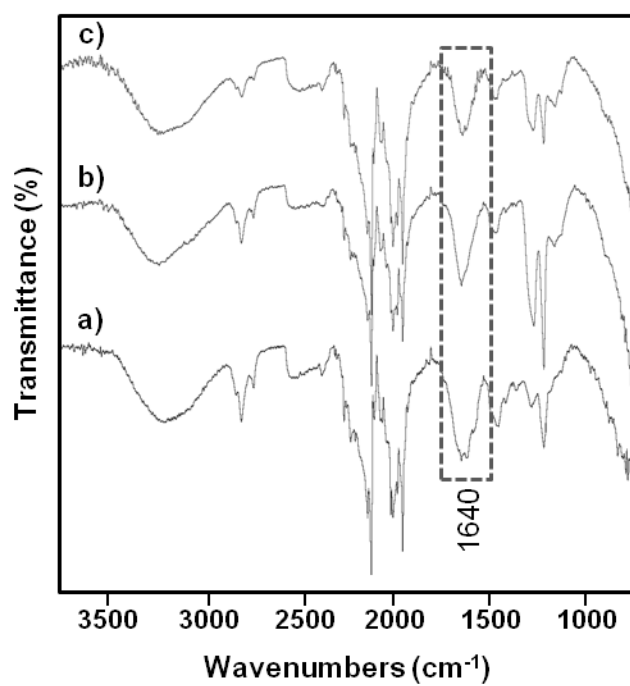
Figure 3.7 ATR-FITR spectra of a) f-NS, b) f-NR and c) f-NP.

CHAPTER 4

Cytotoxicity, cellular uptake and membrane association of
the three different shaped UCNPs

In this chapter, we reported the cytotoxicity of sphere, rod and hexagonal prism shaped UCNPs obtained from previous chapter (Chapter 3) using normal and cancer cell lines. The effect of particles shape on cellular uptake and membrane association was also studied in detail.

4.1 Experimental details

4.1.1 Culture medium and chemical reagent for cell culture and treatment

Dulbecco's modified Eagle's medium (DMEM), Roswell Park Memorial Institute (RPMI) 1640 medium, fetal bovine serum (FBS), sodium pyruvate, 4-(2-hydroxyethyl)-1-piperazineethanesulfonic acid (HEPES), L-glutamine and trypsin-1 mM EDTA were supplied by Hyclone (UT, USA). Penicillin was purchased from General Drugs House Co., Ltd. (Bangkok, Thailand). Streptomycin was purchased from M & H Manufacturing Co., Ltd. (Samut Prakan, Thailand). Advanced Minimum Essential medium was supplied by Gibco (NY, USA), 3-(4,5-dimethylthiazol-2-yl)-2,5-diphenyltetrazolium bromide (MTT) was purchased from USB Corporation (OH, USA). 4′,6-diamidino-2-phenylindole (DAPI) was purchased from life technologies (OR, USA). Paraformaldehyde was purchased from Sigma-Aldrich (Steinheim, Germany). Dimethyl sulfoxide (DMSO) was obtained from RCI Labscan (Bangkok, Thailand).

4.1.2 Cell culture

The A-375 human melanoma cell line (ATCC CRL-1619) was provided by the American Type Culture Collection (ATCC) (Manassas, VA, USA). A-375 cells were cultured in complete medium containing DMEM supplemented with 10% v/v FBS, 100mM sodium pyruvate, 10 mM HEPES, 100 U/mL penicillin and 0.4 mg/mL

streptomycin. The cells were maintained in a humidified atmosphere containing 5% CO_2 at 37 ℃ (Thermoelectron 311 incubator) and harvested using 0.25% w/v trypsin-1 mM EDTA.

The HepG2 human liver carcinoma cell line (ATCC HB-8065) was provided by ATCC. HepG2 cells were cultured in complete medium containing RPMI-1640 medium supplemented with 10% v/v FBS, 100 mM sodium pyruvate, 10 mM HEPES, 100 U/mL penicillin and 0.4 mg/mL streptomycin. The cells were maintained in a humidified atmosphere containing 5% CO_2 at 37 ℃ (Thermoelectron 311 incubator) and harvested using 0.25% w/v trypsin-1 mM EDTA.

The WI-38 human lung normal cell line (ATCC CCL-75) was provided by the ATCC. WI-38 cells were cultured in complete medium containing advanced-MEM supplemented with 5% v/v FBS, 200 mM L-glutamine, 100 U/ml penicillin and 0.4 mg/ml streptomycin. The cells were maintained in a humidified atmosphere containing 5% CO_2 at 37 ℃ (Thermoelectron 311 incubator) and harvested using 0.25% w/v trypsin-1 mM EDTA.

4.1.3 *In vitro* cytotoxicity assay

The *in vitro* cytotoxicity of COOH-PEG-UCNPs was determined on cancer cells and normal cells using MTT assay. A-375 cells, HepG2 cells and WI-38 cells were seeded in a 96-well plates as a density of 6×10^3 cells per well and cultured in 100 µL of complete medium at 37 °C under 5% CO_2 atmosphere overnight. Then, cell culture medium in each well was replaced by 100 µL of complete medium containing COOH-PEG-NS, COOH-PEG-NR and COOH-PEG-NP with concentration ranging from 1000 to 3 µg/mL. The cells were incubated for 24 h at 37 °C under 5% CO_2. Subsequently, 10 µL of MTT solution (5 mg/mL in phosphate buffer saline (PBS)) was added to each well and incubated for additional 4 h at 37 °C and 5% CO_2. The medium was gently removed and replaced with 200 µL of DMSO to dissolve the formazan crystals. The

absorbance of dissolved formazan was measured at the wavelength of 540 nm by an Anthos 2010 microplate reader (Biochrom Ltd., Cambridge, UK). The cell viability can be calculated using the below formula:

Cell viability (%) = (Absorbance of tested cells/Absorbance of control cells) x100

The cells in complete medium with no tested samples were used as controls and set as 100%. All samples were tested in triplicate wells, and two independent experiments were performed.

4.1.4 Cellular association study

- Confocal laser scanning fluorescence microscopy (CLFM)

A-375 cells were seeded in an 8-wells cell culture black chamber slide as a density of 6×10^3 cells per well, cultured in 200 µL of complete medium and incubated at 37 °C under 5% CO_2 overnight. Subsequently, the culture medium was removed and replaced by 200 µL of f-UCs (f-NS, f-NR and f-NP) at concentration of 500 µg/mL in complete medium. The cells were incubated for additional 6 h at 37 °C, 5% CO_2 and then washed gently three times with cold PBS to remove unbound particles. Cell imaging was employed by an Eclipse-C1 Ti Series confocal laser scanning fluorescence microscope (Nikon, Tokyo, Japan) using excitation wavelength of 488 nm and detection at 525 nm.

HepG2 cells were seeded in an 8-wells cell culture black chamber slide as a density of 1×10^4 cells per well, cultured in 200 µL of complete medium and incubated at 37 °C under 5% CO_2 overnight. Subsequently, the culture medium was removed and replaced by 200 µL of f-UCs (f-NS, f-NR and f-NP) at the concentration of 500 µg/mL in complete medium. The cells were incubated for additional 6 h at 37 °C, 5% CO_2. At the end of incubation, the cells were washed gently three times with cold PBS,

fixed by 4% w/v paraformaldehyde, washed three times with PBS, and then nuclei stained with DAPI followed by wash with PBS three times. Cell imaging was employed by CLFM.

- Flow cytometry analysis

The A-375 and HepG2 cells were used to investigate the effect of shape of UCNPs on cellular uptake. The cells were seeded in a 24-well plates as a density of 1.5×10^5 cells per well, cultured in 500 µL of complete medium and incubated at 37 $^{\circ}$C under 5% CO_2 overnight. Then, the culture medium was removed and replaced by 500 µL of f-NS, f-NR and f-NP at concentration of 500 µg/mL in complete medium. The cells were incubated with particles over a time ranging from 1 to 6 h at 37 $^{\circ}$C, 5% CO_2. At the end of incubation time, the cells were triply washed with cold PBS pH 7.4 to remove unbound particles and collected by cell scraper. Subsequently, cell suspension was centrifuged at 3,000 rcf for 5 min at 4 $^{\circ}$C, and the cell pellet was resuspended in cold PBS before subjected to analyze using flow cytometry. Intracellular detection was performed by a Cytomics FC500MPL (Becman Coulter Inc., NY, USA) flow cytometer using laser with excitation wavelength of 488 nm and detection through fluorescence channel 1 (FL1) at 525 nm. In each sample, at least 10,000 cells were counted. The cells in complete medium with no samples were used as controls. The acquired data were processed by FlowJo software (Tree Star, Inc.) using the mean fluorescence tool. Statistical data were analyzed by one-way ANOVA and LSD using SPSS software. A p value of <0.01 was considered statistical significance.

4.1.5 Preparation of lipid bilayer membrane

Cell-sized liposomes were prepared using dioleoyl L-α phosphatidylcholine (DOPC) purchased from Avanti Polar Lipids (Alabaster, AL, USA). Twenty microliters of 2 mM lipid in chloroform was mixed with 12 µL of 10 mM glucose in methanol. The mixed solution was dried in glass vial by nitrogen gas flow to form a thin film, and the

film was kept for 3 h under vacuum. The liposomes were obtained after hydration the film with 200 µL of MilliQ water for 2-3 h at 37 °C. The obtained liposomes were incubated with f-NS, f-NR and f-NP before subjected to confocal laser microscope (Olympus FV-1000, Japan). The fluorescence intensity of the particles on liposome surface was measured by the Image J software.

4.2 *In vitro* cytotoxicity

The cell viability of the COOH-PEG-UCNPs was tested against melanoma cell (A-375), cancer liver cell (HepG2) and normal lung cell (WI-38) by MTT assay. The viability of the untreated cells was set as 100% and the viability of three shapes of COOH-PEG-UCNPs treated cells was relatively calculated. After 24 h of incubation, the cell viability of all three cell lines were greater than 80% even the particles concentration was as high as 1000 µg/mL (Figure 4.1). Therefore, it could be concluded that COOH-PEG-UCNPs exhibited a low cytotoxicity against cancer and normal cell lines. Interestingly, among three shapes of particles at concentrations of 1000 µg/mL, toxicity of nanorod was significantly higher than nanosphere and nanoprism. These results suggested that the cytotoxicity of the UCNPs is shape dependent, and the highest toxicity for rod shape particles have been reported by previous studies.[50-52]
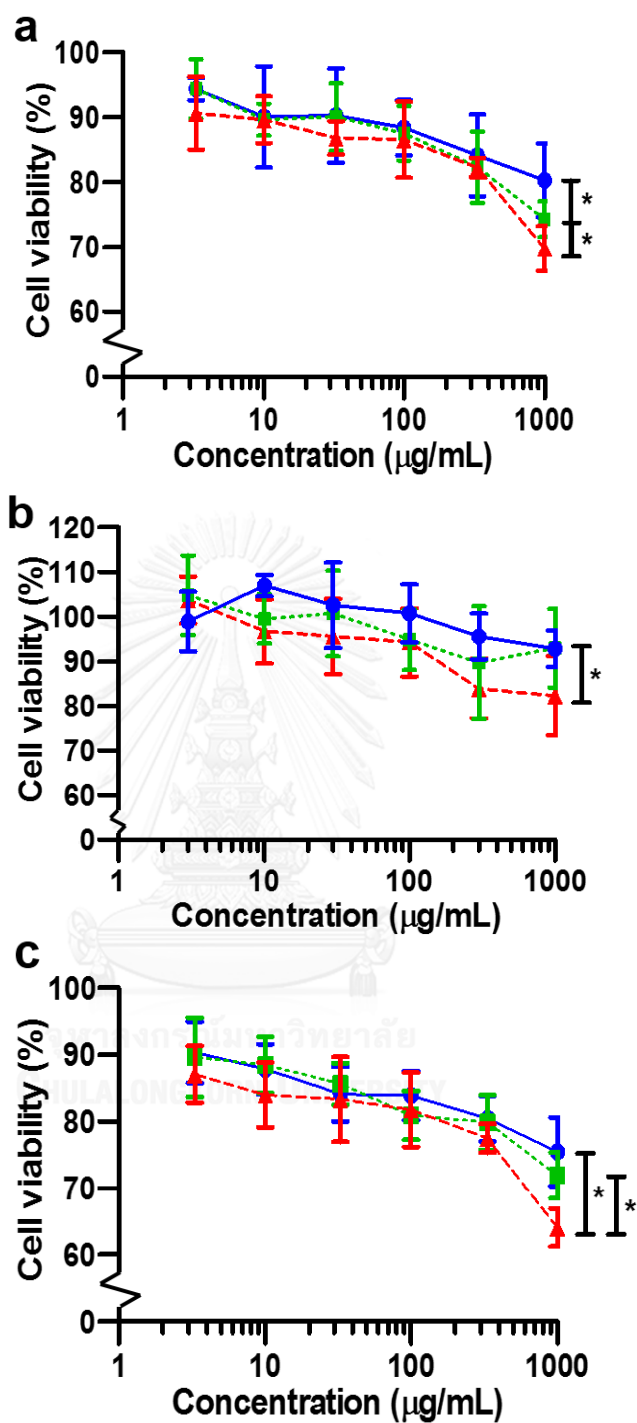
Figure 4.1 *In vitro* cytotoxicity of COOH-PEG-NS (circle), COOH-PEG-NR (triangle) and COOH-PEG-NP (square) against a) A-375, b) HepG2 and c) WI-38 cell lines at incubation time of 24 h. Data represent means $\pm$ SD (n = 6). Statistical significant difference was considered using one-way ANOVA and LSD (*p < 0.01).

4.3 Particle-Cell association

There are several studies indicated that higher toxicity was associated with higher degrees of cellular uptake.[50, 52] We investigated the shape effect of UCNPs on cellular uptake. Confocal laser scanning fluorescence microscope (CLSM) was performed to observe the cellular uptake of the three different shaped UNPCs into A-375 and HepG2 cell lines. Figure 4.2a showed the CLSM images of A-375 cells incubated with f-NS, f-NR and f-NP for 6 h. Fluorescence signal from the fluorescent labeled nanoparticles was observed in the cells with a high signal-to-background ratio while the control cells incubated without the nanoparticles showed no fluorescence signal under similar imaging parameters and conditions. All particles were observed at cytoplasmic region, as indicated by green fluorescence. Moreover, the CLSM images showed that more intense of green fluorescence could be detected in the A-375 cells exposed to f-NR than that in those exposed to f-NS and f-NP under the same conditions. It was clearly evidenced that at 6 h of incubation much more f-NR had been taken up comparing with f-NS and f-NP. The same results were also observed in HepG2 (Figure 4.2b).
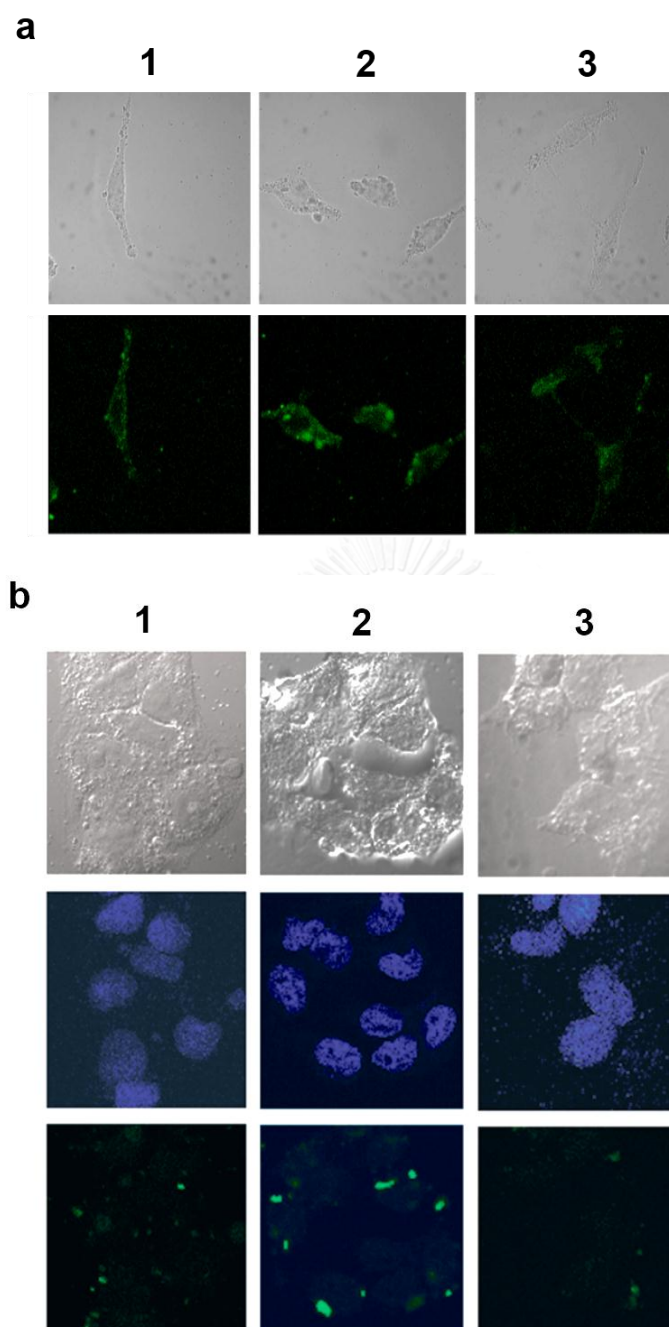
Figure 4.2 Representative confocal laser scanning fluorescence microscopy (CLSM) images of a) A-375 and b) HepG2 cells incubated with f-NS (column 1), f-NR (column 2) and f-NP (column 3) at 37 °C for 6h. Upper panel represents differential interference contrast (DIC) mode, middle panel represents DAPI stained nucleus and lower panel represents fluorescent emission of particles.

To support this incident, quantitative experiment using flow cytometry was also carried out. The f-NS, f-NR and f-NP were incubated with A-375 and HepG2 cells, and the cellular uptake was quantitatively evaluated at different incubation time points. Fluorescein molecules content per unit mass of f-UCNPs was quantified and used to normalize flow cytometry results so that the degree of cellular uptake among the three shapes of particles could be directly compared. The mean fluorescence intensity (MFI) of f-UCNPs was displayed as a relative value with untreated cells (MFI = 1.0). As seen in Figure 4.3a, the increase of incubation time from 1 h to 6 h led to an enhance the cellular interaction between cells and all three shaped particles, thus indicating that cellular uptake was time dependent. The amount of f-NR associated with A-375 cell was significantly higher than that of f-NS and f-NP for all of the time of investigation. More importantly, the results obtained from HepG2 cells also exhibited the same trend (Figure 4.3b). It was therefore implied that rod shaped particles had the highest degree of particle–cell association, and thus they were taken up into the cell efficiently. These results were in good agreement with a study on cell viability, suggesting that cellular uptake was strongly depended on the particles shape. The effect of particle shapes on cellular uptake was also previously published by Li and coworkers [52] which indicated that 10-hydroxycamptothecin nanorods showed higher *in vitro* and *in vivo* anti-cancer activity than that of nanospheres.
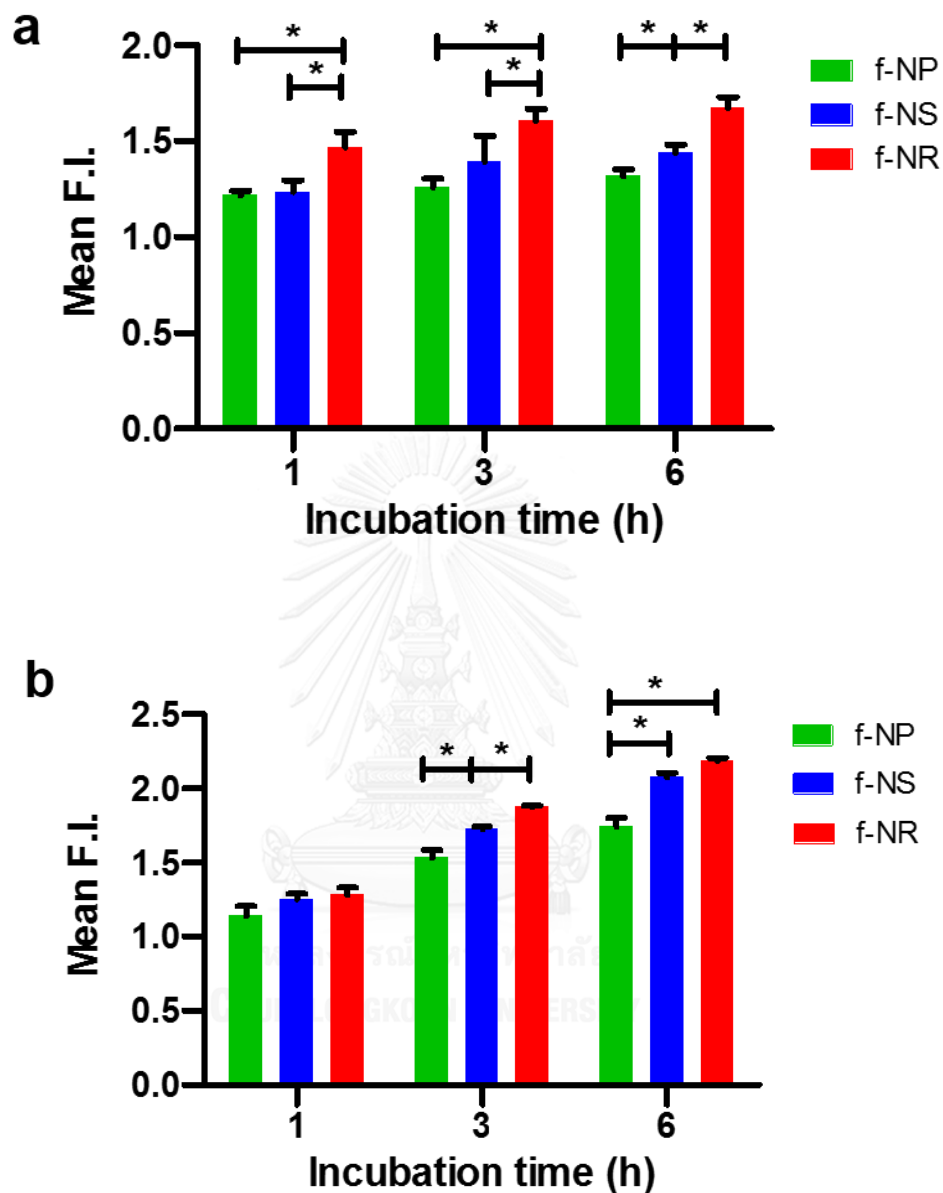
Figure 4.3 Cellular uptake behavior. Plots of fluorescence intensity (F.I.) from flow cytometry detection in a) A-375 and b) HepG2 cells after incubation with the three shaped f-UCNPs at difference time points. Data represent means ± SD (n = 6, from two independent experiments). Statistical significant difference was considered using one-way ANOVA and LSD (*p < 0.01).

4.4 Particle-lipid bilayer membrane association

To better understand how cellular association is related to particle morphology, lipid bilayer membrane of artificially made cell-sized liposome was considered as a model. Cell-sized liposomes with liquid-disordered phase were constructed using dioleoyl L-α phosphatidylcholine (DOPC).[53] The f-NS, f-NR and f-NP were then incubated with cell-sized liposome for 20 min, and the initial association with lipid bilayer membrane was compared by measuring the relative amounts of particles bound to the lipid bilayer membrane of the liposomes using confocal laser microscopy (λ_{ex} = 488 and λ_{em} = 525 nm). Under the same instrument setting, the f-NS and f-NR showed some fluorescent signal on the membrane surface, whereas no fluorescent signal was detected for f-NP (Figure 4.4). It is interesting that the f-NR exhibited the highest fluorescent intensity on the membrane surface compared with other two shapes. In addition, the f-NS showed slightly association with the membrane, whereas no any adhesion could be observed for the f-NP (Figure 4.4). These results clearly indicated that the degree of lipid bilayer membrane association was highest for rod shaped particles, followed by the sphere and hexagonal prism shaped particles. We explain the difference in membrane affinity of different shaped particles through the theory of membrane curvature.[54-56]
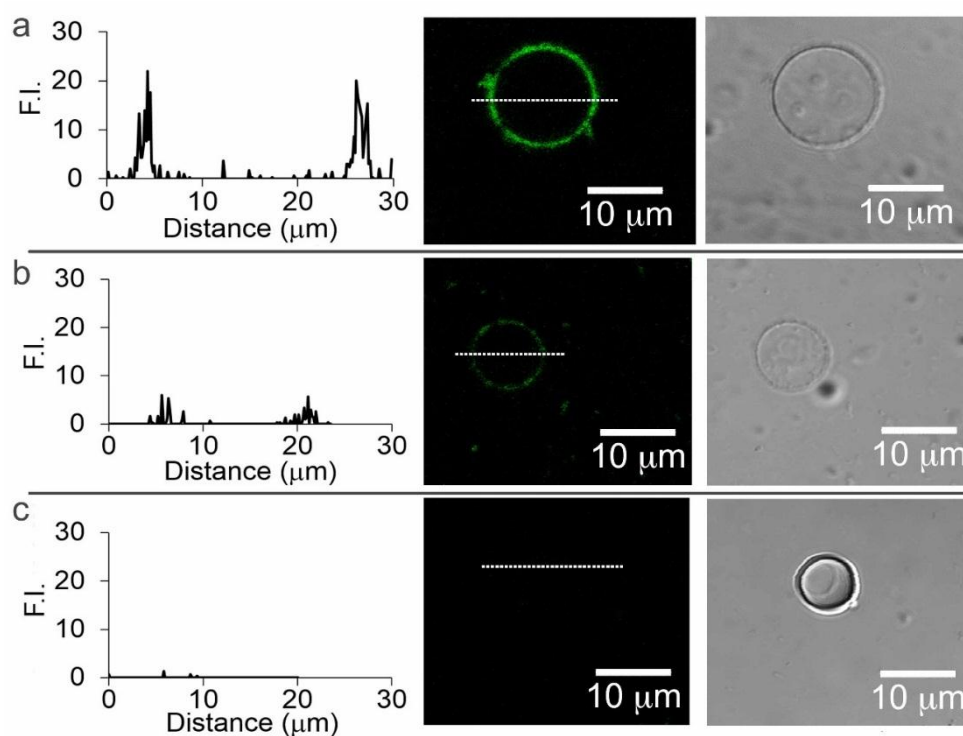
Figure 4.4 Association of the three shaped f-UCNPs on liposomes. Plots of fluorescence intensity (F.I.) of a) f-NS, b) f-NR and c) f-NP along the white dashed line of the corresponding liposome shown on the right of the graph. The differential interference contrast images of the corresponding liposomes are shown next to the fluorescence images.

Base on the theory of membrane curvature, an association of particle on the membrane surface allows the membrane curvature which is the curving of membrane to wrap the particle. Shape of the particles strongly affects the membrane curvation. The hexagonal prism shaped particles possesses a lot of sharp edges which may cause the difficulty in curvature of the membrane, leading to non-preferable association. This explains the minimal adhesion of the prism-shaped particles to the membrane found in our experiment. When the spherical and rod particles adhere on the membranes, they are partially wrapped with angles θ_1 and θ_2 (Figure 4.5). The adhesion surface areas for the sphere (A_{sph}) and the rod (A_{rod}) are given by [57]:

$$A_{\text{sph}} = 2\pi R^2 (1 - \cos\theta_1),$$

$$A_{\text{rod}} = 2\pi R^2 (1 - \cos\theta_2) + LR\theta_2.$$

The free energy of the membrane association for the sphere (F_{sph}) and the rod (F_{rod}) can be calculated using the following equation [57]:

$$F_{sph} = 4\pi K_b (1 - \cos\theta_1),$$

$$F_{rod} = 4\pi K_b (1 - \cos\theta_2) + \frac{\pi}{8} K_b (x - 1),$$

where x is the aspect ratio of rods (x=b/a=1+L/2R)

and K_b is the bending modulus of the membrane.

Figure 4.5 showed the difference of the free energies plotted as a function of aspect ratio (x), when the spherical and rod particles adhere on the membrane with the same surface area ($A_{sph}=A_{rod}$) and θ_2 is assumed to constant at value of $\pi/4$. Corresponding to our experimental results, the rod had x=1.5 whereas x=1 was observed for the spherical particle. At the aspect ratio of the two shapes, it is found that the adhesion of the rod is more stable than that of the sphere.
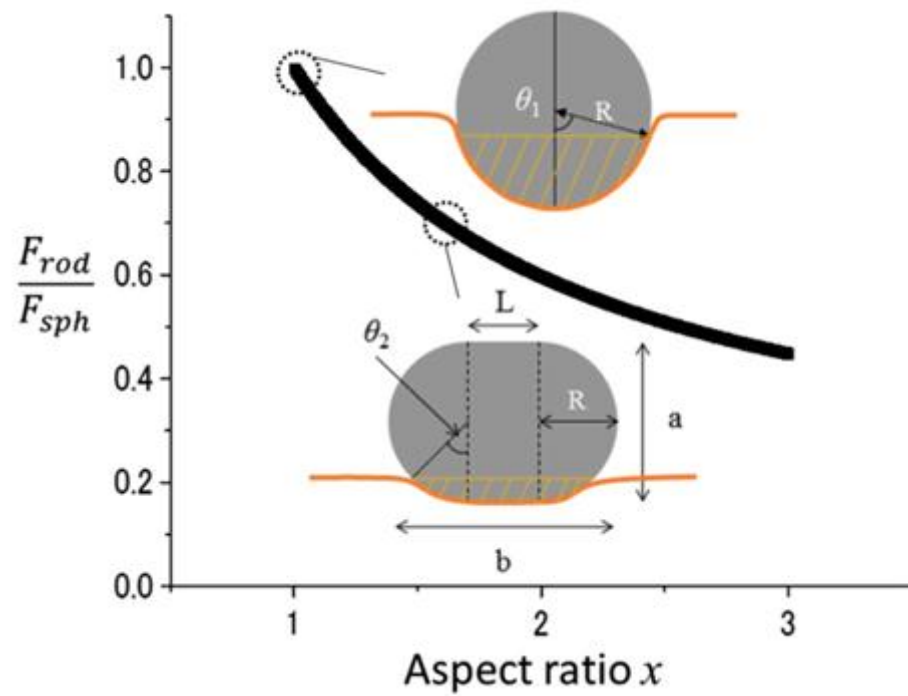
Figure 4.5 Free energy of the membrane that wraps spherical and rod particles as a function of aspect ratio.

CHAPTER 5

Synthesis, characterization and surface modification of core/shell-UCNPs and their upconversion emission properties

In this chapter, $NaYF_4$:Yb^{3+}, Tm^{3+} core structure UCNPs with different doping ratios of Tm^{3+} were synthesized by a thermal decomposition method. To enhance the emission intensity of UCNPs, $NaYF_4$ shell was grown on the surface of core-UCNPs to form a core/shell structure. Then, the core/shell-UCNPs were further surface modified by PEG-diacid to transform their surface from hydrophobic to hydrophilic. The upconversion emission intensity of core-UCNPs, core/shell-UCNPs and PEG-core/shell-UCNPs were compared in detail.

5.1 Experimental details

5.1.1 Chemicals and materials

$YCl_3 \cdot 6H_2O$ (99.99%), $YbCl_3 \cdot 6H_2O$ (99.99%), $TmCl_3 \cdot 6H_2O$ (99.99%), oleic acid (90%), 1-octadecene (90%), ammonium fluoride (NH_4F), sodium hydroxide (NaOH) and Poly(ethylene glycol)bis(carboxymethyl)ether (PEG-diacid, average M_n 600) and 9,10-anthracenediyl-bis(methylene)dimalonic acid (ABDA) were purchased from Sigma-Aldrich (Steinheim, Germany). Methanol and ethanol were purchased from Merck (Darmstadt, Germany). All chemicals were used as received without any further purification.

5.1.2 Synthesis of $NaYF_4$:Yb^{3+}, Tm^{3+} (core-UCNPs)

In a typical procedure, the desired amount of $YCl_3 \cdot 6H_2O$, $YbCl_3 \cdot 6H_2O$ and $TmCl_3 \cdot 6H_2O$ were added in a three-neck round-bottom flask with the presence of oleic acid (24 mL) and octadecene (60 mL). The mixture was stirred and heated to 130 °C for 40 min under vacuum until form a homogeneous solution. After the solution temperature was cooled down to room temperature (30 °C), NaOH (10 mmol) and

NH$_4$F (16 mmol) in methanol (20 mL) was added drop-wise to the obtained solution and continuously stirred for 40 min. The mixed solution was then heated at 75 °C to evaporate the methanol. Subsequently, the reaction temperature was rapidly increased to 300 °C and maintained at this temperature for 90 min under the gentle nitrogen gas flow. The resulting solution was cooled down to room temperature and precipitated by addition of ethanol. To collect the nanocrystals, the precipitates were centrifuged (GL21M Changsha Yingtai instrument, China) at 5000 rpm (2688 rcf) and washed several times with ethanol.

5.1.3 Synthesis of NaYF$_4$:Yb^{3+}, Tm^{3+}/NaYF$_4$ UCNPs (core/shell-UCNPs)

To grow of the shell layer, YCl$_3$·6H$_2$O (2.0 mmol) was added into a three-neck round-bottom flask with the presence of oleic acid (12 mL) and octadecene (30 mL). The reaction mixture was heated to 130 °C with magnetic stirring for 40 min under vacuum. When reaction temperature was cooled down to 80 °C, the dispersion of core structure nanocrystals in chloroform was allowed to add under nitrogen atmosphere to act as seed crystals. The mixed solution was heated to 110 °C in order to remove the chloroform and then cooled down to 50 °C. A methanol solution (20 mL) containing sodium hydroxide (5.0 mmol) and ammonium fluoride (8.0 mmol) was added into the reaction solution and continuously stirred for 30 min. The reaction solution was slowly heated to 75 °C to remove the methanol and then rapidly heated to 300 °C and maintained at this temperature for 90 min under the nitrogen gas flow. The obtained solution was cooled down to room temperature and precipitated by addition of ethanol. The precipitations were centrifuged (GL21M Changsha Yingtai instrument, China) at 5000 rpm (2688 rcf) and followed by wash several times with ethanol.

5.1.4 Synthesis of water dispersible core/shell-UCNPs (COOH-PEG-UCNPs)

The core/shell-UCNPs (50 mg) were added into a glass vial with the presence of ethanol (5 mL) and PEG-600-diacid (125 mg). The vial was capped, sonicated, heated at 75 $^{\circ}$C and maintained at this temperature overnight. The dispersion was left to cool down at room temperature before addition of hexane to precipitate the particles. The PEG coated core/shell UCNPs were collected by centrifugation at 8000 rpm (6880 rcf) and washed several times with ethanol.

5.2 Characterization

5.2.1 Core structure UCNPs (core-UCNPs)

The core structure $NaYF_4$ co-doped with 30 mol% Yb^{3+}, x mol% Tm^{3+} (x = 0.2, 0.5, 1.0 and 1.5) UCNPs were synthesized by a thermal decomposition method in the presence of oleic acid and octadecene at 300 $^{\circ}$C. The contents of Y^{3+}, Yb^{3+} and Tm^{3+} in each sample were quantitatively determined using inductively coupled plasma optical emission spectrometry (ICP-OES) technique and the results are shown in Table 5.1. The ICP-OES analysis of samples indicated that the concentrations of trivalent cations in the final products were in good agreement with the original molar ratios of the added precursors.

Table 5.1 The relative contents of metal in the core structure β-NaYF$_4$: Yb^{3+}, Tm^{3+} UCNPs.

Nanoparticle	Y^{3+} (mol%)	Yb^{3+} (mol%)	Tm^{3+} (mol%)
NaYF$_4$: 30 mol% Yb^{3+}, 0.2 mol% Tm^{3+}	71.58±5.67	28.15±5.66	0.27±0.02
NaYF$_4$: 30 mol% Yb^{3+}, 0.5 mol% Tm^{3+}	69.71±0.11	29.71±0.13	0.58±0.04
NaYF$_4$: 30 mol% Yb^{3+}, 1.0 mol% Tm^{3+}	68.61±0.14	30.15±0.10	1.24±0.07
NaYF$_4$: 30 mol% Yb^{3+}, 1.5 mol% Tm^{3+}	69.81±0.08	28.51±0.16	1.68±0.09

The crystal structure of as-synthesized core-UCNPs was investigated by X-ray diffraction (XRD) technique. As shown in Figure 5.1, all diffraction peaks could be matched with the standard reference pattern of β-NaYF$_4$ (JCPDS file no. 28-1192), confirming that all nanocrystals were of hexagonal phase.
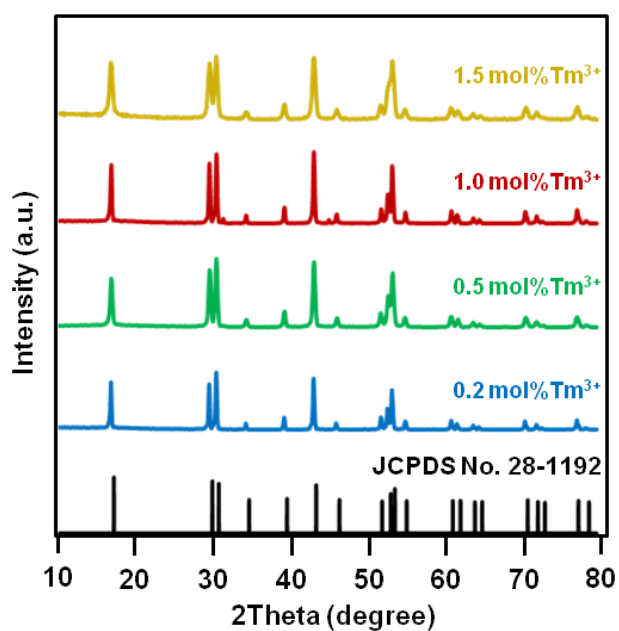
Figure 5.1 XRD patterns of core structure NaYF$_4$: 30 mol% Yb^{3+}, x mol% Tm^{3+} UCNPs with different Tm^{3+} ratios (x= 0.2, 0.5, 1.0 and 1.5).

Upconversion emissions of β-NaYF$_4$: Yb^{3+}, Tm^{3+} UCNPs with different doping ratios of Tm^{3+} (0.2, 0.5, 1.0 and 1.5 mol%) with constant Yb^{3+} content at 30 mol% are shown in Figure 5.2. Under a 980 nm diode laser excitation, all β-NaYF$_4$: Yb^{3+}, Tm^{3+} UCNPs exhibits emission in UV, visible and NIR regions. The first region is the UV where emission peaks at 290, 350 and 365 nm are observed. In the visible region, emission peaks are observed at 450, 475 and 650 nm. And, one emission peak at 800 nm is observed in the NIR region. These emission patterns agreed well with previous studies.[4, 58] Although the upconversion emission peak positions depending on the dopant materials do not change, the emission efficiency was affected by different doping concentrations.
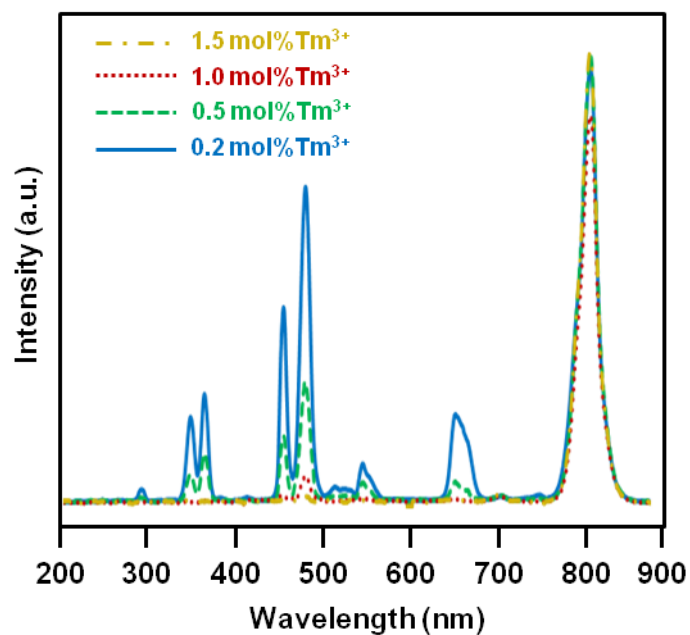
Figure 5.2 Upconversion emission spectra of core structure β-NaYF$_4$: 30 mol% Yb^{3+}, x mol% Tm^{3+} UCNPs with different Tm^{3+} ratios x= 0.2, 0.5, 1.0 and 1.5 in hexane under a 980 nm laser excitation.

When the molar ratio of Tm^{3+} increases from 0.2% to 1.5%, the emission intensities in UV and visible regions decreased. This can be explained by a concentration quenching effect.[59] The increase of Tm^{3+} concentrations results in the decrease of the distance between adjacent Tm ions and the increase of the cross-relaxation that reduces radiative relaxation and thus suppresses the upconversion emission. Moreover, with the increasing Tm doping concentrations, the excitation energy obtained by each Tm ion would also be decreased and resulted in the weakening emission.

5.2.2 Core/shell structure UCNPs (core/shell-UCNPs)

The β-NaYF$_4$: 30 mol% Yb^{3+}, 0.2 mol% Tm^{3+} was selected as a core particle for construction of core/shell structured UCNPs because it gave the highest upconversion emission in UV and visible regions. The core/shell structure could be constructed by controlling the nucleation and growth of nanocrystals. The β-NaYF$_4$: 30 mol% Yb^{3+}, 0.2 mol% Tm^{3+} core nanocrystals served as nuclei for the NaYF$_4$ shell growing on their surface. This led to formation of β-NaYF$_4$: 30 mol% Yb^{3+}, 0.2 mol% Tm^{3+}/ NaYF$_4$ core/shell structure UCNPs (core/shell-UCNPs). The XRD pattern of the obtained core/shell-UCNPs was in a good agreement with the standard pattern of β-NaYF$_4$ (JCPDS file no. 28-1192), confirming that these nanocrystals remain in a pure hexagonal phase (Figure 5.3).
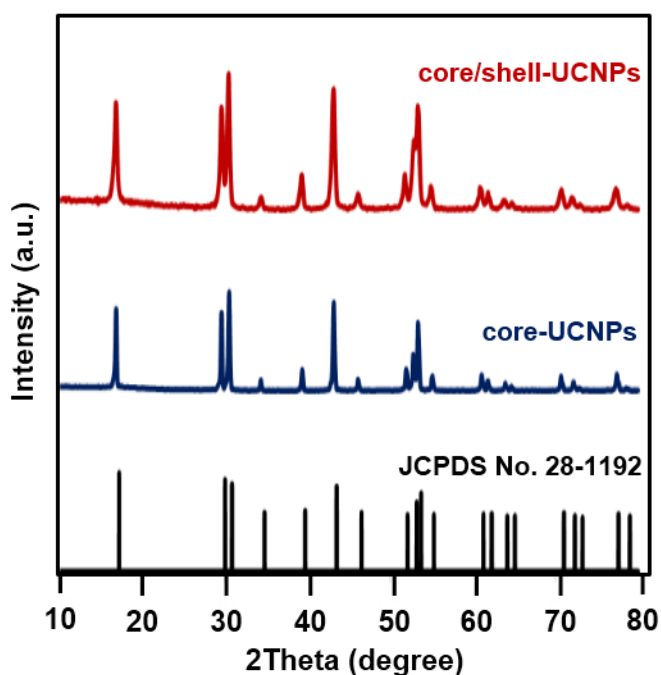
Figure 5.3 XRD patterns of a) core-UCNPs and b) core/shell-UCNPs.

5.2.3 PEG coated core/shell-UCNPs (PEG-UCNPs)

To allow the core/shell-UCNPs to disperse in water for application in biology, original oleate ligands were replaced by PEG-diacid ligands using a ligand exchange strategy. The PEG coating makes them dispersible in water. The functional groups existing on the surface of nanocrystals were characterized by ATR-FTIR. After ligand exchange, the particles exhibited two peaks at 1635 and 1441 cm^{-1} in their IR spectrum, assignable to the asymmetric and symmetric stretching vibrations of carboxylate forms (COO$^-$), respectively. The absorption peak at 1747 cm^{-1} was also presented due to the free carboxylic groups. Additionally, the new peak at 1043 cm^{-1}, assigned to the C-O-C stretching vibration of ethylene glycol could be observed (Figure 5.4). These results confirmed the attachment of PEG on the surface of the PEG-coated core/shell structure upconverting nanoparticles (PEG-UCNPs). The zeta potential value of -25.9±2.97 mV for the PEG-UCNPs agrees well with the existence of negatively charged carboxylic groups on their surface.
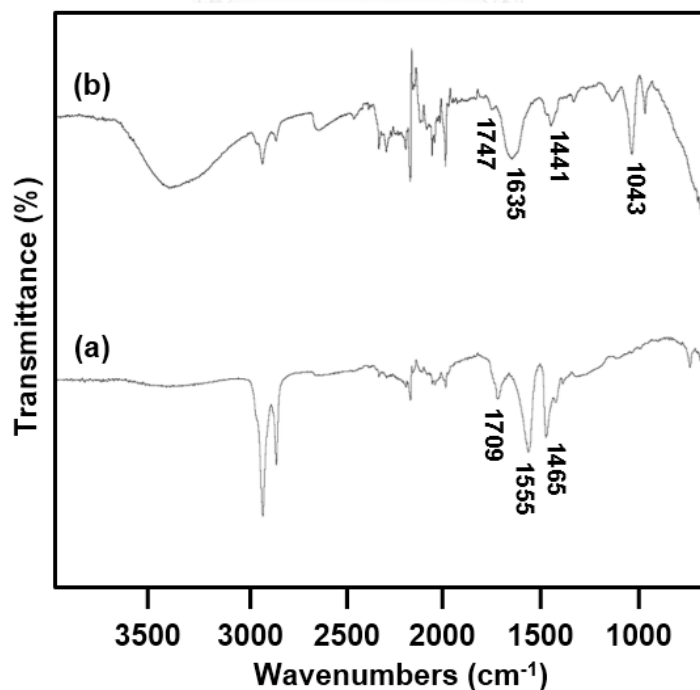
Figure 5.4 ATR-FTIR spectra of a) core/shell-UCNPs and b) PEG-UCNPs.

Morphology of the obtained nanocrystals was observed by transmission electron microscopy (TEM) (Figure 5.5). The core/shell-UCNPs showed an elongated-spherical shape with an average length/width of 30.74 ± 1.22/23.36 ± 0.75 nm (aspect ratio ~1.3), larger than the original core-UCNPs (a spherical shape with 17.49 ± 2.10 nm in size). This observation could be used for supporting the achievement of the core/shell construction. Furthermore, TEM image of the PEG-UCNPs still showed the same particle shape and size, comparing with core/shell-UCNPs. This clearly indicated that exchanging of oleate ligands into COOH-PEO-COOH ligands did not significantly affect the shape and size of the nanocrystals.
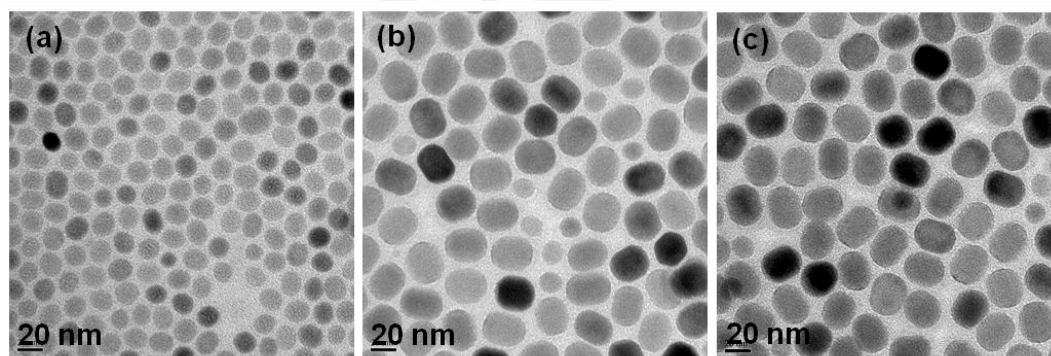
Figure 5.5 Representative TEM images of a) core-UCNPs b) core/shell-UCNPs and c) PEG-UCNPs.

The upconversion emission spectra of suspended nanocrystals (1000 µg/mL) under a 980 nm laser excitation at 4 W are shown in Figure 5.6. When the β-NaYF$_4$: 30 mol% Yb^{3+}, 0.2 mol% Tm^{3+} core nanocrystals were surrounded by β-NaYF$_4$ shells, the upconversion emission intensity was obviously increased which was similar to the article reported by Yi and co-workers.[19] This is because the energy losses at the nanocrystals surfaces are protected by the β-NaYF$_4$ shell. Furthermore, the upconversion emission intensity of PEG-UCNPs (after ligand exchange) was not much reduced comparing with that of the core/shell-UCNPs. From all above information, it

can be noted that the ligand exchange strategy did not affect their morphology and optical property.
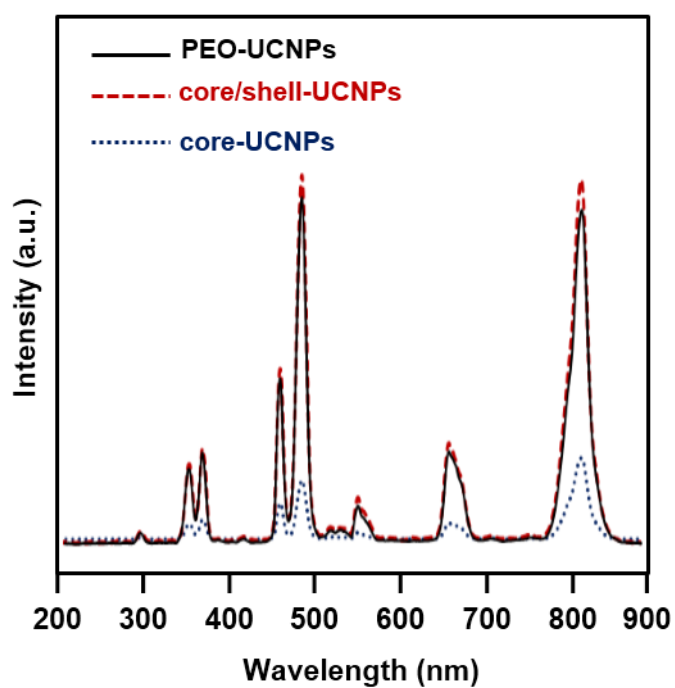
Figure 5.6 Upconversion emission spectra of a) core-UCNPs in hexane, b) core/shell-UCNPs in hexane and c) PEG-UCNPs in water at concentration of 1000 µg/mL under 4 W of a 980 nm laser excitation.

CHAPTER 6

Photosensitizer loaded core/shell-UNPCs and their application in antibacterial photodynamic therapy

In this chapter, the resulting PEG coated core/shell-UCNPs (PEG-UCNPs) from previous chapter (Chapter 5) were loaded with photosensitizer having an absorption matches with the emission of PEG-UCNPs. The cytotoxicity and singlet oxygen production of the obtained particles were studied. The effectiveness of photosensitizer loaded UCNPs was demonstrated through photodynamic therapy of *Propionibacterium acnes* (*P.acnes*).

6.1 Experimental method

6.1.1 Synthesis of photosensitizer, *meso*-Tetraphenyltetrabenzo-porphyrinatozinc (ZnTPTBP)

The photosensitizer, *meso*-Tetraphenyltetrabenzoporphyrinatozinc (ZnTPTBP) was kindly obtained from Associate Professor Dr. Patchanita Thamyongkit (Department of chemistry, Chulalongkorn University). The chemical structure of ZnTPTBP was shown as below.
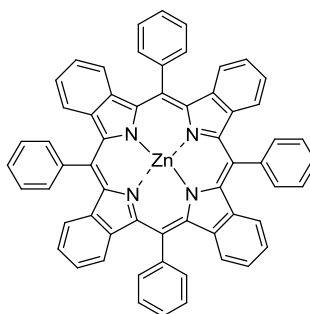
ZnTPTBP

ZnTPTBP as a green powder (95% purity). ^{1}H-NMR δ7.17 (dd, J = 6.0, 3.2 Hz, 8H), 7.29 (dd, J = 6.0, 3.2 Hz, 8H), 7.87 (t, J = 7.2 Hz, 8H), 7.95 (t, J = 7.2 Hz, 4H), 8.31 (d, J = 7.2 Hz, 8H); MALDI-TOF-MS m/z obsd 875.598[M$^+$], calcd 876.223 [M =

$C_{60}H_{36}N_4Zn$]; λ_{abs} (ε, toluene) 470 (1.9×10^5), 613, 656 nm; λ_{em} (λ_{ex} = 470 nm, toluene) 666, 731 nm.

6.1.2 Loading of photosensitizer onto PEG-UCNPs (ZnTPTBP-UCNPs)

Thirty microliter of ZnTPTBP in DMSO solution (1 mg/mL) was added into an aqueous suspension of UCNPs (1 mg/mL). The mixed solution was vortexed for 30 min at room temperature. The loading content of ZnTPTBP on UCNPs was evaluated using direct and indirect method. For former method, suspension of ZnTPTBP-UCNPs was centrifuged, and the precipitate was then analyzed by ICP-OES. To evaluate the amount of unloaded ZnTPTBP for latter method, the suspension was centrifuged, and then the free ZnTPTBP in supernatant was determined using an Optizen Pop QX UV–Vis spectrophotometer (Mecasys, South Korea). Thus, the amount of ZnTPTBP on the UCNPs could be estimated by subtracting the unloaded amount from the original amount.

6.1.3 Singlet oxygen measurement

Each of tested samples including PEG-UCNPs (0.5 mg), ZnTPTBP (15 µL of 1 mg/mL of ZnTPTBP in DMSO) and ZnTPTBP-UCNPs (0.5 mg) was added in 1 mL of milliQ water containing 10 µM of 9,10-anthracenediyl-bis(methylene)dimalonic acid (ABDA) dye. The dispersion of tested sample containing 10 µM of ABDA dye together with 10 mM of sodium azide, singlet oxygen scavenger, was used as a control sample. The mixture was placed in 1 mL quartz cuvette and then irradiated with a 980 nm laser at 8 W/cm^2 beginning from time 0 to 70 seconds. The intensity of fluorescence emission of ABDA (λ_{em} = 430 nm and λ_{ex} = 380 nm) was recorded using a fluorescence spectrophotometer. The same experiment was performed with no laser irradiation. Each data point reported as mean ± SD from two independent experiments.

6.1.4 Culture medium and chemical reagent for cell culture and treatment

Dulbecco's modified Eagle's medium (DMEM), fetal bovine serum (FBS), sodium pyruvate, 4-(2-hydroxyethyl)-1-piperazineethanesulfonic acid (HEPES), and trypsin-1 mM EDTA were supplied by Hyclone (UT, USA). Penicillin was purchased from General Drugs House Co., Ltd. (Bangkok, Thailand). Streptomycin was purchased from M & H Manufacturing Co., Ltd. (Samut Prakan, Thailand). 3-(4,5-dimethylthiazol-2-yl)-2,5-diphenyltetrazolium bromide (MTT) was purchased from USB Corporation (OH, USA).

6.1.5 Cell culture

The A-375 melanoma cell (ATCC CRL-1619) was provided by ATCC. A-375 cells were cultured in DMEM supplemented with 10% v/v FBS, 100 mM sodium pyruvate, 10 mM HEPES, 100 U/ml penicillin and 0.4 mg/ml streptomycin at 37 $^{\circ}$C under 5% CO_2 atmosphere (Thermoelectron 311 incubator)

6.1.6 *In vitro* cytotoxicity assay

Cell viability of PEG-UCNPs and ZnTPTBP-UCNPs with and without NIR irradiation was evaluated by MTT assay. A-375 cells were seeded in a 96-well plates as a density of 8×10^3 cells per well and cultured in 100 μL of complete medium at 37 $^{\circ}$C under 5% CO_2 atmosphere overnight. Then, one hundred microliter of complete medium containing tested samples such as PEG-UCNPs and ZnTPTBP-UCNPs was added to obtain the final concentration of 1000 - 3 μg/mL. The cells in complete medium with no tested samples were served as controls. For non-NIR irradiation condition, the cells were incubated at 37 $^{\circ}$C under 5% CO_2 for 24 h. But, for NIR irradiation condition, cells were incubated with tested samples for 4 h, then exposed to NIR at 560 J/cm^2 and finally incubated until complete 24 h. Subsequently, 10 μL of MTT solution (5 mg/mL in PBS) was added to each well and incubated for additional 4 h at 37 $^{\circ}$C and 5% CO_2. The medium was gently removed and replaced with 200 μL of DMSO to dissolve the formazan crystals. The absorbance of dissolved formazan was

measured at the wavelength of 540 nm by a Microplate reader (Anthos 2010, Biochrom Ltd., UK). Each concentration was performed in triplicate wells and two independent experiments were performed.

6.1.7 Bacterial strain and culture media

Propionibacterium acnes or *P. acnes* (DMST 14916) was obtained by the Department of Medical Sciences, Nonthaburi, Thailand. Brain heart infusion (BHI) broth and BHI agar were purchased from Difco laboratories (MI, USA). Generbox anaer systems were supplied by Biomerieux (Marcy l'Etoile, France).

6.1.8 Bacterial culture

P. acnes was incubated in BHI broth at 37 ^{o}C for 72 h under anaerobic conditions using BiomerieuxGasPak systems. The absorbance at 600 nm was measured by a microplate reader to estimate bacterial growth, and bacterial suspension was then adjusted to yield approximately 1.5×10^8 colony-forming units (CFU)/mL with fresh medium.

6.1.9 *In vitro* antimicrobial photodynamic therapy

The experiment was tested in sterile 96-well plates. Fifty microliter of a tested sample including PEG-UCNPs, ZnTPTBP and ZnTPTBP-UCNPs was added into each well containing 50 µL of the bacterial suspension in BHI broth. Control well contained bacterial suspension while negative control well contained only bacterial medium. Each tested condition was repeated in triplicate. After incubation at 37 ^{o}C under anaerobic conditions for 4 h, the wells were irradiated with a 980 nm laser at power density of 8 W/cm^2 from time 0 to 60 seconds. The laser was vertically located 5 cm above the well plate. The well plates were then reincubated at the same condition until complete 72 h. To determine the growth of *P. acnes,* five microliter of p-iodonitrotetrazolium violet (INT) (4 mg/mL) were added to each well, and waiting until a color change was observed. The minimum inhibitory concentrations (MIC) were

defined as the lowest concentration of a test sample that inhibited the *P. acnes* growth, as indicated by no color change after INT adding. To evaluate the minimum bactericidal concentrations (MBC), a loopful of bacterial suspension from each well was plated on BHI agar. The agar plates were incubated at 37 °C for 72 h under anaerobic conditions, and then colonies of *P. acnes* were counted. The MBC were defined as the lowest concentration of a tested sample that prevented the *P. acnes* growth, as indicated by no bacterial colonies after subculture on a BHI agar plate.

6.2 Characterization and emission properties of ZnTPTBP-UCNPs

A photosensitizer ZnTPTPB was loaded onto the PEG-UCNPs. In order to prove that ZnTPTBP was certainly loaded onto the UCNPs, suspensions of free ZnTPTBP, PEG-diacid polymer mixed with ZnTPTBP and the UNPCs mixed with ZnTPTBP were prepared and then centrifuged at 10,000 rcf for 5 min. It was found that no precipitate was observed for free ZnTPTBP and PEG-diacid mixed with ZnTPTBP samples after centrifugation whereas green precipitate was observed for the mixture of ZnTPTBP and the UCNPs. This observation indicated the successful loading of ZnTPTBP onto UCNPs, which was pulled down by the centrifugation force. The loading capacity of ZnTPTBP was 2.3% and 3%, analyzed by ICP-OES and UV-vis spectroscopy, respectively.

To evidence the energy transfer between UCNPs and the loaded ZnTPTBP, the upconversion emission of ZnTPTBP loaded UCNPs was measured under a 980 nm laser excitation. As shown in Figure 6.1, the fluorescence emission intensities at 450, 475 and 635 nm of PEG-UCNPs was higher than that of ZnTPTBP-UCNPs. The obvious decrease of emission intensities in visible region (450-500 nm) was noticed after ZnTPTBP loading. This is due to the energy transfer from the UCNPs to the loaded ZnTPTBP molecules, which have a high intense absorption at 430-490 nm. The decrease at 635 nm was less pronounced regarding to the small absorption at 635 nm of ZnTPTBP. Moreover, the small decrease was also observed for emission peaks at 360 and 365

nm. This is probably due to a small absorption tail in the UV region of the ZnTPTBP. These results strongly confirm that radiations emitted from the UCNPs under a 980 nm laser excitation, can be efficiently absorbed by the loaded ZnTPTBP.
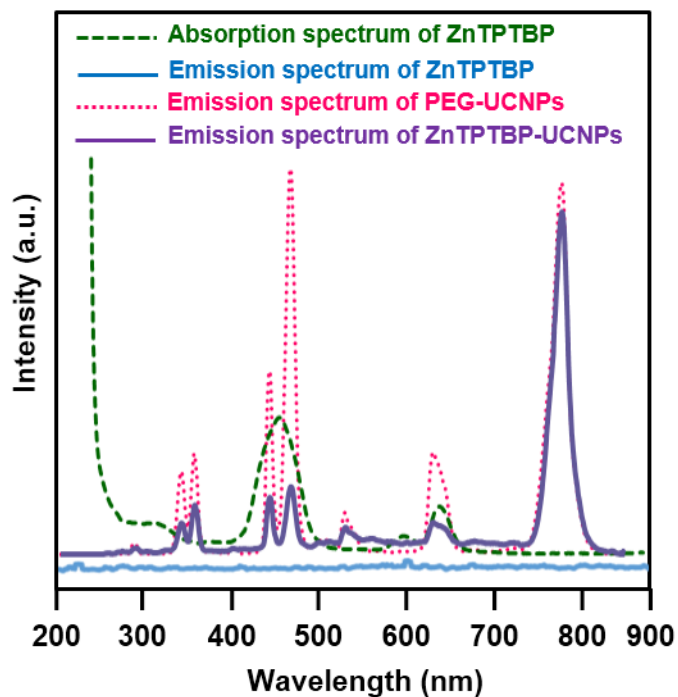
Figure 6.1 Absorption spectrum of ZnTPTBP, and emission spectra of ZnTPTBP, PEG-UCNPs and ZnTPTBP-UCNPs when excitation with a 980 nm laser at power density of 8 W/cm^2.

6.3 Singlet oxygen production

To determine the production of singlet oxygen in our system, the aqueous suspension of PEG-UCNPs, ZnTPTBP and ZnTPTBP-UCNPs was irradiated with a 980 nm laser at power density of 8 W/cm^2 in the presence of fluorescence probe 9,10-anthracenediyl-bis(methylene)dimalonic acid (ABDA).[60] Basically, when the ABDA reacts with the singlet oxygen, it will be in an endoperoxide form which leads to a decrease of fluorescence intensity. Thus, the presence of singlet oxygen production can be monitored by measuring the fluorescence emission of ABDA at wavelength of 430 nm when excitation at 380 nm. As shown in Figure 6.2, the results revealed that

decrease of mean fluorescence intensity of ABDA with the increasing time of NIR irradiation was observed for all samples. Interestingly, there were an obvious and gradual decrease of fluorescence intensity of ABDA in case of ZnTPTBP-UCNPs and PEG-UCNPs, respectively. To confirm the decrease of fluorescence intensity was a result of the produced singlet oxygen, the singlet oxygen scavenger, sodium azide (NaN$_3$) was added to the suspension of all samples. Under the same condition, the mean fluorescence intensity of ABDA remains unchanged even being NIR irradiation at various times. It should be noted that the singlet oxygen can be produced from ZnTPTBP-UCNPs and PEG-UCNPs under laser irradiation and the amount of singlet oxygen increased with increasing irradiation time.
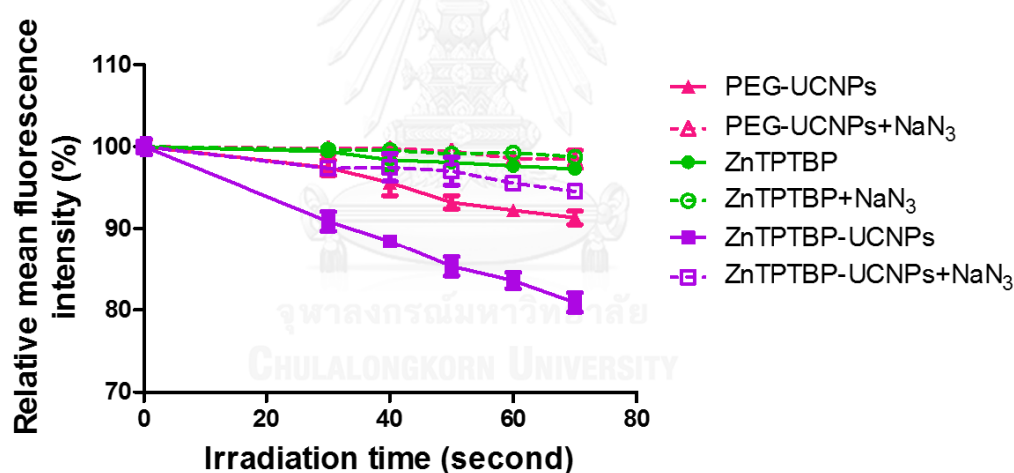
Figure 6.2 Fluorescence intensity of ABDA mixed PEG-UCNPs, ZnTPTBP, ZnTPTBP-UCNPs, PEG-UCNPs + NaN$_3$, ZnTPTBP + NaN$_3$ and ZnTPTBP-UCNPs + NaN$_3$ after being a 980 nm laser irradiation at 8 W/cm^2 with various time points (λ_{em} = 430 nm and λ_{ex} = 380 nm).

6.4 *In vitro* cytotoxicity

To assess the biocompatibility of PEG-UCNPs and ZnTPTBP-UCNPs, A-375 cells were incubated with a tested sample and the cell viability after 24 h was determined

using MTT assay. Under no NIR irradiation, all tested samples showed no significant effect on viability of the A-375 cells even at the concentrations of up to 500 µg/mL (Figure 6.3). These results suggest that PEG-UCNPs and ZnTPTBP-UCNPs can be considered to have a low cytotoxicity. Upon the NIR exposure at 560 J/cm^2, the cytotoxicity of the ZnTPTBP-UCNPs at 500 µg/mL was more pronounced than that of PEG-UCNPs (Figure 6.3). These results agrees well with a better ability of ZnTPTBP-UCNPs to produce singlet oxygen for killing cells upon NIR irradiation.
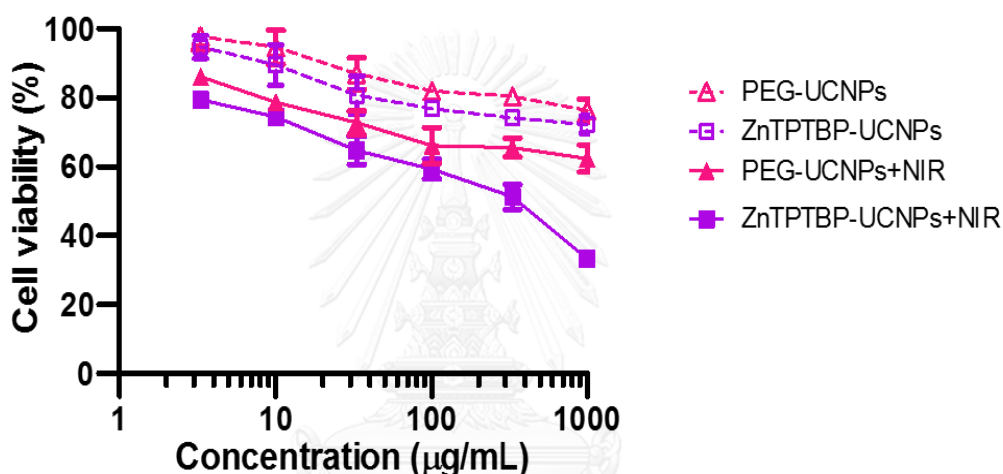
Figure 6.3 *In vitro* cytotoxicity of PEG-UCNPs (triangle) and ZnTPTBP-UCNPs (square) against A-375 cells after 24 h of incubation. Data represent mean ± SD (n = 6) from two independent experiments. Without NIR irradiation, cell viability of ZnTPTBP-UCNPs was not significantly different from that of PEG-UCNPs, considered by Mann Whitney U test at the P value of ≤ 0.05. However, Mann-Whiney U test indicated significantly lower cell viability of ZnTPTBP-UCNPs + NIR comparing with PEG-UCNPs + NIR, at the P value ≤ 0.05.

6.5 Anti-*P. acnes* photodynamic therapy

There is evidence that the singlet oxygen has involved in *P. acnes* eradication,[61] and photo-excitation of bacterial porphyrins themselves has been also

reported for killing bacteria.[62, 63] Base on water dispersible character, non-toxic nature, UVA emissions that match with the absorption range of *P. acnes* porphyrins and effective singlet oxygen production upon NIR irradiation of the ZnTPTBP-UCNPs, thus, we expected that combination of ZnTPTBP-UCNPs and NIR light could be used for the anti-*P. acnes* photodynamic therapy. To prove this assumption, *in vitro* anti-*P. acnes* activity of the material under NIR irradiation was studied in detail.

Growth of *P. acnes* after irradiation with a 980 nm laser was first studied. The experiments were carried out by bacterial broth method and the viable bacteria after irradiation were determined using p-Iodonitrotetrazolium violet (INT). The suspensions of ZnTPTBP (concentration of 15 µg/mL), UCNPs (concentration of 500 µg/mL) and ZnTPTBP-UCNPs (concentration of 500 µg/mL for UCNPs and 15 µg/mL for ZnTPTBP) were prepared and then treated with *P. acnes*. We observed no inhibitory effects on *P. acnes* growth in treatment without laser irradiation (radiant exposure = 0 J/cm^2) (Table 6.1). Irradiation was carried out with a 980 nm laser at power density of 8 W/cm^2 for various irradiation times. Laser irradiation alone did not affect the growth of *P. acnes.* The same result was observed when ZnTPTBP was used (Table 6.1). Irradiation times of 30, 40, 50 and 60 seconds corresspond to the radiant exposures of 240, 320, 400 and 480 J/cm^2, respectively. However, in the presence of either the PEG-UCNPs or the ZnTPTBP-UCNPs, inhibition of *P. acnes* growth was observed under appropriate NIR irradiation ennergy (Table 6.1). Comparing these two samples at the same particles concentration, ZnTPTBP-UCNPs need less NIR radiation. The result suggested that ZnTPTBP-UCNPs were more effective than PEG-UCNPs for inhibiting the growth of *P. acnes*. This is because at similar NIR exposure ZnTPTBP-UCNPs could produce more singlet oxygen than PEG-UCNPs (discussed in above experiment).

Table 6.1 *P. acnes* growth at various times of irradiation with a 980 nm laser.

Samples	Radiant exposures (J/cm^2)				
	0	240	320	400	480
Water	-	-	-	-	-
ZnTPTBP (15 µg/mL)	-	-	-	-	-
PEG-UCNPs (500 µg/mL)	-	-	-	-	+
ZnTPTBP-UCNPs (15 µg/mL ZnTPTBP, 500 µg/mL PEG-UCNPs)	-	-	-	+	+

(**-**) = uninhibited growth and (**+**) = inhibited growth

The photodynamic therapy against *P. acnes* was further investigated to evaluate the minimum inhibitory concentrations (MIC) and the minimum bactericidal concentrations (MBC) values. The irradiation condition was fixed at radiant exposure of 560 J/cm^2 (8 W/cm^2, 70 second), and the concentrations of samples were varied by two-fold serial dilution. The MIC value against *P. acnes* after irradiation of PEG-UCNPs was 500 µg/mL whereas the MIC of ZnTPTBP-UCNPs was 250 µg/mL for PEG-UCNPs and 7.5 for ZnTPTBP (Table 6.2). Moreover, the MBC values were also evaluated. The MBC value of PEG-UCNPs was 1000 µg/mL while the MBC of ZnTPTBP-UCNPs was 500 µg/mL for PEG-UCNPs and 15 µg/mL for ZnTPTBP (Table 6.2). These results correspond to our assumption that ZnTPTBP-UCNPs should provide a lower MIC and MBC values than the PEG-UCNPs. Therefore, we conclude that ZnTPTBP-UCNPs are more effective than PEG-UCNPs in photo-treatment of *P. acnes*.

Table 6.2 The photodynamic therapy of *P. acnes* at 980 nm, radiant exposure of 560 J/cm^2.

Sample	MIC (µg/mL)	MBC (µg/mL)
PEG-UCNPs	500	1000
ZnTPTBP-UCNPs	PEG-UCNPs = 250	PEG-UCNPs = 500
	ZnTPTBP = 7.5	ZnTPTBP = 15

CHAPTER 7

Conclusion

NaYF$_4$ co-doped with 30 mol% Yb^{3+} and 0.5 mol% Tm^{3+} upconverting nanoparticles (UCNPs) have been successfully synthesized using a thermal decomposition method in the presence of octadecene and oleic acid as a solvent and a ligand, respectively. Adjustment of the volume ratio of ligand and solvent can cause the formation of three different shaped UCNPs, including nanosphere, nanorod and nanoprism. All three shaped UCNPs exhibit an ability to disperse in water, and have the same crystal phase structure and surface charge. Cytotoxicity in cancer human cells (A-375 and HepG2) and normal human cell (WI-38), degree of cellular uptake into A-375 and HepG2 cells, and degree of lipid bilayer membrane association are highest for the rod-shaped UCNPs. Free energy of lipid bilayer membrane curvature induced by particle association is lower for the rods comparing to the spheres, while the sharp edge of the prism-shaped particles prevents stable membrane curving. Therefore, the most stable membrane curvature induced by the rod particles is the main driving force for their high degree of membrane association which results in more cellular uptake and higher cytotoxicity.

This thesis also demonstrates a near infrared (NIR) light assisted photosensitizer loaded UCNPs on antibacterial photodynamic therapy. The core/shell structured UCNPs based on 0.2mol% Tm^{3+}, 30mol% Yb^{3+}-doped NaYF$_4$/ NaYF$_4$ have been synthesized. The obtained particles show good water dispersibility, non-toxic, hexagonal phase and high UVA and visible emissions. To apply in anti-*P. acnes* photodynamic therapy, *meso*-tetraphenyltetrabenzoporphyrinatozinc (ZnTPTBP) photosensitizer having absorption wavelengths perfectly match with the emission wavelengths of the obtained UCNPs is structural designed, and loaded onto the UCNPs.

The ZnTPTBP loaded UCNPs have an ability to produce singlet oxygen under a 980 nm laser irradiation. *In vitro* anti-*P. acnes* activity using the obtained particles combined with NIR light reveals that ZnTPTBP loaded UCNPs need less NIR exposure than the unloaded UCNPs, and the MIC and MBC values of the former are lower than latter particles. This work thus introduces an alternative strategy for acnes treatment through the combination of the bio-transparent NIR light and the bio-compatible photosensitizer loaded UCNPs.

REFERENCES

[1]   Yi, G., Lu, H., Zhao, S., Ge, Y., Yang, W., Chen, D., and Guo, L. H. Synthesis, characterization, and biological application of size-controlled nanocrystalline NaYF$_4$:Yb,Er infrared-to-visible up-conversion phosphors. Nano Letters 4(11) (2004): 2191-2196.

[2]   Wang, F. and Liu, X. Recent advances in the chemistry of lanthanide-doped upconversion nanocrystals. Chemical Society Reviews 38(4) (2009): 976-989.

[3]   Xiong, L.-Q., Chen, Z.-G., Yu, M.-X., Li, F.-Y., Liu, C., and Huang, C.-H. Synthesis, characterization, and in vivo targeted imaging of amine-functionalized rare-earth up-converting nanophosphors. Biomaterials 30(29) (2009): 5592-5600.

[4]   Boyer, J.C., Carling, C.J., Gates, B.D., and Branda, N.R. Two-way photoswitching using one type of near-infrared light, upconverting nanoparticles, and changing only the light intensity. Journal of the American Chemical Society 132(44) (2010): 15766-15772.

[5]   Haase, M. and Schäfer, H. Upconverting nanoparticles. Angewandte Chemie - International Edition 50(26) (2011): 5808-5829.

[6]   Wang, F., Banerjee, D., Liu, Y., Chen, X., and Liu, X. Upconversion nanoparticles in biological labeling, imaging, and therapy. Analyst 135(8) (2010): 1839-1854.

[7]   Wang, F., Chatterjee, D.K., Li, Z., Zhang, Y., Fan, X., and Wang, M. Synthesis of polyethylenimine/NaYF$_4$ nanoparticles with upconversion fluorescence. Nanotechnology 17(23) (2006): 5786-5791.

[8]   Boyer, J.-C., Vetrone, F., Cuccia, L.A., and Capobianco, J.A. Synthesis of colloidal upconverting NaYF$_4$ nanocrystals doped with Er^{3+}, Yb^{3+} and Tm^{3+}, Yb^{3+} via thermal decomposition of lanthanide trifluoroacetate precursors. Journal of the American Chemical Society 128(23) (2006): 7444-7445.

[9]   Liang, X., Wang, X., Zhuang, J., Peng, Q., and Li, Y. Synthesis of NaYF$_4$ nanocrystals with predictable phase and shape. Advanced Functional Materials 17(15) (2007): 2757-2765.

[10] Zhang, F., Li, J., Shan, J., Xu, L., and Zhao, D. Shape, Size, and phase-controlled rare-earth fluoride nanocrystals with optical up-conversion properties. <u>Chemistry – A European Journal</u> 15(41) (2009): 11010-11019.

[11] Krämer, K.W., Biner, D., Frei, G., Güdel, H.U., Hehlen, M.P., and Lüthi, S.R. Hexagonal sodium yttrium fluoride based green and blue emitting upconversion phosphors. <u>Chemistry of Materials</u> 16(7) (2004): 1244-1251.

[12] Yi, G.-S. and Chow, G.-M. Colloidal LaF_3:Yb,Er, LaF_3:Yb,Ho and LaF_3:Yb,Tm nanocrystals with multicolor upconversion fluorescence. <u>Journal of Materials Chemistry</u> 15(41) (2005): 4460-4464.

[13] Lim, S.F., Riehn, R., Ryu, W. S., Khanarian, N., Tung, C.-K., Tank, D., and Austin, R. H. *In Vivo* and scanning electron microscopy imaging of upconverting nanophosphors in *Caenorhabditis elegans.* <u>Nano Letters</u> 6(2) (2005): 169-174.

[14] Sun, Q., Zhao, H., Chen, X., Wang, F., Cai, W., and Jiang, Z. Upconversion emission enhancement in silica-coated Gd_2O_3:Tm^{3+}, Yb^{3+} nanocrystals by incorporation of Li^+ ion. <u>Materials Chemistry and Physics</u> 123(2–3) (2010): 806-810.

[15] Suyver, J.F., Grimm, J., Van Veen, M.K., Biner, D., Krämer, K.W., and Güdel, H.U. Upconversion spectroscopy and properties of $NaYF_4$ doped with $Er^{3+,}$ Tm^{3+} and/or Yb^{3+}. <u>Journal of Luminescence</u> 117(1) (2006): 1-12.

[16] Zhou, J., Liu, Z., and Li, F. Upconversion nanophosphors for small-animal imaging. <u>Chemical Society Reviews</u> 41(3) (2012): 1323-1349.

[17] Yi, G.S. and Chow, G.M. Synthesis of hexagonal-phase $NaYF_4$:Yb,Er and $NaYF_4$:Yb,Tm nanocrystals with efficient up-conversion fluorescence. <u>Advanced Functional Materials</u> 16(18) (2006): 2324-2329.

[18] Vetrone, F., Boyer, J.-C., Capobianco, J.A., Speghini, A., and Bettinelli, M. Significance of Yb^{3+} concentration on the upconversion mechanisms in codoped Y_2O_3:Er^{3+},Yb^{3+} nanocrystals. <u>Journal of Applied Physics</u> 96(1) (2004): 661-667.

[19] Yi, G.S. and Chow, G.M. Water-soluble $NaYF_4$:Yb,Er(Tm)/$NaYF_4$/polymer core/shell/shell nanoparticles with significant enhancement of upconversion fluorescence. <u>Chemistry of Materials</u> 19(3) (2007): 341-343.

[20]   Mai, H.-X., Zhang, Y.-W., Sun, L.-D., and Yan, C.-H. Highly efficient multicolor up-conversion emissions and their mechanisms of monodisperse NaYF$_4$:Yb,Er core and core/shell-structured nanocrystals. The Journal of Physical Chemistry C 111(37) (2007): 13721-13729.

[21]   Vetrone, F., Naccache, R., Mahalingam, V., Morgan, C.G., and Capobianco, J.A. The active-core/active-shell approach: A strategy to enhance the upconversion luminescence in lanthanide-doped nanoparticles. Advanced Functional Materials 19(18) (2009): 2924-2929.

[22]   Wang, Y., Tu, L., Zhao, J., Sun, Y., Kong, X., and Zhang, H. Upconversion luminescence of β-NaYF$_4$: Yb^{3+}, Er^{3+}@β-NaYF$_4$ core/shell nanoparticles: excitation power density and surface dependence. The Journal of Physical Chemistry C 113(17) (2009): 7164-7169.

[23]   Boyer, J.-C., Manseau, M.-P., Murray, J.I., and van Veggel, F.C.J.M. Surface modification of upconverting NaYF$_4$ nanoparticles with PEG–phosphate ligands for NIR (800 nm) biolabeling within the biological window. Langmuir 26(2) (2009): 1157-1164.

[24]   Chen, Z., Chen, H., Hu, H., Yu, M., Li, F., Zhang, Q., Zhou, Z., Yi, T., and Huang, C. Versatile synthesis strategy for carboxylic acid–functionalized upconverting nanophosphors as biological labels. Journal of the American Chemical Society 130(10) (2008): 3023-3029.

[25]   Cheng, L., Yang, K., Zhang, S., Shao, M., Lee, S., and Liu, Z. Highly-sensitive multiplexed in vivo imaging using pegylated upconversion nanoparticles. Nano Research 3(10) (2010): 722-732.

[26]   Wang, L., Yan, R., Huo, Z., Wang, L., Zeng, J., Bao, J., Wang, X., Peng, Q., and Li, Y. Fluorescence resonant energy transfer biosensor based on upconversion-luminescent nanoparticles. Angewandte Chemie International Edition 44(37) (2005): 6054-6057.

[27]   Sivakumar, S., Diamente, P.R., and van Veggel, F.C.J.M. Silica-coated Ln^{3+}-doped LaF$_3$ nanoparticles as robust down- and upconverting biolabels. Chemistry – A European Journal 12(22) (2006): 5878-5884.

[28]   Liu, Q., Chen, M., Sun, Y., Chen, G., Yang, T., Gao, Y., Zhang, X., and Li, F. Multifunctional rare-earth self-assembled nanosystem for tri-modal upconversion luminescence /fluorescence /positron emission tomography imaging. Biomaterials 32(32) (2011): 8243-8253.

[29]   Chatterjee, D.K., Gnanasammandhan, M.K., and Zhang, Y. Small upconverting fluorescent nanoparticles for biomedical applications. Small 6(24) (2010): 2781-2795.

[30]   Wang, M., Mi, C.-C., Wang, W.-X., Liu, C.-H., Wu, Y.-F., Xu, Z.-R., Mao, C.-B., and Xu, S.-K. Immunolabeling and NIR-excited fluorescent imaging of HeLa cells by using NaYF$_4$:Yb,Er upconversion nanoparticles. ACS Nano 3(6) (2009): 1580-1586.

[31]   Yu, M., Li, F., Chen, Z., Hu, H., Zhan, C., Yang, H., and Huang, C. Laser scanning up-conversion luminescence microscopy for imaging cells labeled with rare-earth nanophosphors. Analytical Chemistry 81(3) (2009): 930-935.

[32]   Liu, Q., Sun, Y., Li, C., Zhou, J., Li, C., Yang, T., Zhang, X., Yi, T., Wu, D., and Li, F. ^{18}F-labeled magnetic-upconversion nanophosphors via rare-earth cation-assisted ligand assembly. ACS Nano 5(4) (2011): 3146-3157.

[33]   Niu, X., Chen, H., Wang, Y., Wang, W., Sun, X., and Chen, L. Upconversion fluorescence-SERS dual-mode tags for cellular and in Vivo imaging. ACS Applied Materials & Interfaces 6(7) (2014): 5152-5160.

[34]   He, L., Feng, L., Cheng, L., Liu, Y., Li, Z., Peng, R., Li, Y., Guo, L., and Liu, Z. Multilayer dual-polymer-coated upconversion nanoparticles for multimodal imaging and serum-enhanced gene delivery. ACS Applied Materials & Interfaces 5(20) (2013): 10381-10388.

[35]   Jayakumar, M.K.G., Idris, N.M., and Zhang, Y. Remote activation of biomolecules in deep tissues using near-infrared-to-UV upconversion nanotransducers. Proceedings of the National Academy of Sciences 109(22) (2012): 8483-8488.

[36]   Gai, S., Yang, P., Li, C., Wang, W., Dai, Y., Niu, N., and Lin, J. Synthesis of magnetic, up-conversion luminescent, and mesoporous core–shell-structured nanocomposites as drug carriers. Advanced Functional Materials 20(7) (2010): 1166-1172.

[37]   Fedoryshin, L.L., Tavares, A.J., Petryayeva, E., Doughan, S., and Krull, U.J. Near-infrared-triggered anticancer drug release from upconverting nanoparticles. ACS Applied Materials & Interfaces 6(16) (2014): 13600-13606.

[38]   Chatterjee, D.K. and Yong, Z. Upconverting nanoparticles as nanotransducers for photodynamic therapy in cancer cells. Nanomedicine 3(1) (2008): 73-82.

[39]   Wang, C., Tao, H., Cheng, L., and Liu, Z. Near-infrared light induced *in vivo* photodynamic therapy of cancer based on upconversion nanoparticles. Biomaterials 32(26) (2011): 6145-6154.

[40]   Idris, N.M., Gnanasammandhan, M.K., Zhang, J., Ho, P.C., Mahendran, R., and Zhang, Y. *In vivo* photodynamic therapy using upconversion nanoparticles as remote-controlled nanotransducers. Nature Medicine 18(10) (2012): 1580-1585.

[41]   Cui, S., Yin, D., Chen, Y., Di, Y., Chen, H., Ma, Y., Achilefu, S., and Gu, Y. *In vivo* targeted deep-tissue photodynamic therapy based on near-infrared light triggered upconversion nanoconstruct. ACS Nano 7(1) (2013): 676-688.

[42]   Wang, H., Liu, Z., Wang, S., Dong, C., Gong, X., Zhao, P., and Chang, J. MC540 and upconverting nanocrystal coloaded polymeric liposome for near-infrared light-triggered photodynamic therapy and cell fluorescent imaging. ACS Applied Materials & Interfaces 6(5) (2014): 3219-3225.

[43]   Chatterjee, D.K., Rufaihah, A.J., and Zhang, Y. Upconversion fluorescence imaging of cells and small animals using lanthanide doped nanocrystals. Biomaterials 29(7) (2008): 937-943.

[44]   Cao, T., Yang, T., Gao, Y., Yang, Y., Hu, H., and Li, F. Water-soluble $NaYF_4$:Yb/Er upconversion nanophosphors: Synthesis, characteristics and application in bioimaging. Inorganic Chemistry Communications 13(3) (2010): 392-394.

[45]   Hu, H., Xiong, L., Zhou, J., Li, F., Cao, T., and Huang, C. Multimodal-luminescence core–shell nanocomposites for targeted imaging of tumor cells. Chemistry – A European Journal 15(14) (2009): 3577-3584.

[46]   Wang, M., Mi, C., Zhang, Y., Liu, J., Li, F., Mao, C., and Xu, S. NIR-responsive silica-coated $NaYbF_4$:Er/Tm/Ho upconversion fluorescent nanoparticles with tunable emission colors and their applications in immunolabeling and fluorescent

imaging of cancer cells. <u>The Journal of Physical Chemistry C</u> 113(44) (2009): 19021-19027.

[47]   Zhang, P., Steelant, W., Kumar, M., and Scholfield, M. Versatile photosensitizers for photodynamic therapy at infrared excitation. <u>Journal of the American Chemical Society</u> 129(15) (2007): 4526-4527.

[48]   Ungun, B., Prud'homme, R. K., Budijon, S. J., Shan, J., Lim, S. F., Ju, Y., and Austin, R. Nanofabricated upconversion nanoparticles for photodynamic therapy. <u>Opt. Express</u> 17(1) (2009): 80-86.

[49]   Qian, H.S., Guo, H.C., Ho, P.C.-L., Mahendran, R., and Zhang, Y. Mesoporous-silica-coated up-conversion fluorescent nanoparticles for photodynamic therapy. <u>Small</u> 5(20) (2009): 2285-2290.

[50]   Nan, A., Bai, X., Son, S.J., Lee, S.B., and Ghandehari, H. Cellular uptake and cytotoxicity of silica nanotubes. <u>Nano Letters</u> 8(8) (2008): 2150-2154.

[51]   Motskin, M., Wright, D. M., Muller, K., Kyle, N., Gard, T. G., Porter, A. E., and Skepper, J. N. Hydroxyapatite nano and microparticles: Correlation of particle properties with cytotoxicity and biostability. <u>Biomaterials</u> 30(19) (2009): 3307-3317.

[52]   Li, W., Zhang, X., Hao, X., Jie, J., Tian, B., and Zhang, X. Shape design of high drug payload nanoparticles for more effective cancer therapy. <u>Chemical Communications</u> 49(93) (2013): 10989-10991.

[53]   Hamada, T., Morita, M., Miyakawa, M., Sugimoto, R., Hatanaka, A., Vestergaard, M. C., and Takagi, M. Size-dependent partitioning of nano/microparticles mediated by membrane lateral heterogeneity. <u>Journal of the American Chemical Society</u> 134(34) (2012): 13990-13996.

[54]   Galic, M., Jeong, S., Tsai, F.-C., Joubert, L.-M., Wu, Y. I., Hahn, K. M., Cui, Y., and Meyer, T. External push and internal pull forces recruit curvature-sensing N-BAR domain proteins to the plasma membrane. <u>Nat Cell Biol</u> 14(8) (2012): 874-881.

[55]   Dasgupta, S., Auth, T., and Gompper, G. Wrapping of ellipsoidal nano-particles by fluid membranes. <u>Soft Matter</u> 9(22) (2013): 5473-5482.

[56]   Dasgupta, S., Auth, T., and Gompper, G. Shape and orientation matter for the cellular uptake of nonspherical particles. <u>Nano Letters</u> 14(2) (2014): 687-693.

[57]   Tree-Udom, T., Seemork, J., Shigyou, K., Hamada, T., Sangphech, N., Palaga, T., Insin, N., Pan-In, P., and Wanichwecharungruang, S. Shape effect on particle-lipid bilayer membrane association, cellular uptake, and cytotoxicity. ACS Applied Materials & Interfaces 7(43) (2015): 23993-24000.

[58]   Jiang, G., Pichaandi, J., Johnson, N.J.J., Burke, R.D., and van Veggel, F.C.J.M. An effective polymer cross-linking strategy to obtain stable dispersions of upconverting $NaYF_4$ nanoparticles in buffers and biological growth media for biolabeling applications. Langmuir 28(6) (2012): 3239-3247.

[59]   Yin, A., Zhang, Y., Sun, L., and Yan, C. Colloidal synthesis and blue based multicolor upconversion emissions of size and composition controlled monodisperse hexagonal $NaYF_4$: Yb,Tm nanocrystals. Nanoscale 2(6) (2010): 953-959.

[60]   Kuznetsova, N.A., Gretsova, N.S., Yuzhakova, O.A., Negrimovskii, V.M., Kaliya, O.L., and Luk'yanets, E.A. New reagents for determination of the quantum efficiency of singlet oxygen generation in aqueous media. Russian Journal of General Chemistry 71(1) (2001): 36-41.

[61]   Arakane, K., Ryu, A., Hayashi, C., Masunaga, T., Shinmoto, K., Mashiko, S., Nagano, T., and Hirobe, M. Singlet oxygen ($^1\Delta_g$) generation from coproporphyrin in *Propionibacterium acnes* on irradiation. Biochemical and Biophysical Research Communications 223(3) (1996): 578-582.

[62]   Melø, T.B. Uptake of protoporphyrin and violet light photodestruction of *Propionibacterium acnes*. Zeitschrift fur Naturforschung. C, Journal of biosciences 42(1-2) (1987): 123-128.

[63]   Ashkenazi, H., Malik, Z., Harth, Y., and Nitzan, Y. Eradication of *Propionibacterium acnes* by its endogenic porphyrins after illumination with high intensity blue light. FEMS Immunology and Medical Microbiology 35(1) (2003): 17-24.

APPENDIX

Chemical and culture medium preparation

- Phosphate Buffer Saline (PBS) pH 7.4

NaCl (8.00 g), KCl (0.20 g), KH_2PO_4 (0.20 g) and Na_2HPO_4 (1.44 g) were dissolved in distilled water and then adjust volume to 1000 mL. The pH is measured by a pH meter to obtain pH value of 7.4.

- Brain heart infusion (BHI) broth

Seventeen grams of BHI broth was dissolved in 500 mL of reverse osmosis water. The solution was sterilized by autoclaving at 121 ^{o}C at 15 psi for 1 h. Then, the obtained BHI solution was stored at 4 ^{o}C until use.

- Brain heart infusion (BHI) agar

Twenty six grams of BHI agar was dissolved in 500 mL of reverse osmosis water. The solution was sterilized by autoclaving at 121 ^{o}C at 15 psi for 1 h. Then, the BHI agar plate was stored at 4 ^{o}C until use.

VITA

Mr. Thapakorn Tree-udom was born on April 25, 1986 in Samut Sakhon, Thailand. He received a Bachelor's Degree of Science in Chemistry from Kasetsart University in 2008 and a Master's Degree of Science in Petrochemistry and Polymer Science from Chulalongkorn University in 2011. Subsequently, he has started his graduate study a Doctoral degree in Nanoscience and Technology Program, Chulalongkorn University. He had received a scholarship from the Development and Promotion of Science and Technology Talents project (DPST) throughout his study. He also had an opportunity to conduct a research under the supervision of Professor Mark R. Prausnitz at Georgia Institute of Technology, USA for 11 months.

His current address is 49/571 Khok Kham, Muang, Samut Sakhon Thailand 74000.

Publications

1. Tree-Udom, T.; Seemork, J.; Shigyou, K.; Hamada, T.; Sangphech, N.; Palaga, T.; Insin, N.; Pan-In, P.; Wanichwecharungruang, S., Shape Effect on Particle-Lipid Bilayer Membrane Association, Cellular Uptake, and Cytotoxicity. ACS Applied Materials & Interfaces 2015, 7 (43), 23993-24000.

2. Tree-Udom, T.; Thamyongkit, P.; Wiratkasem, N.; Chanchao, C.; Palaga, T.; Insin, N.; Rengpipat, S.; Pienpinijtham, P.; Wanichwecharungruang, S., Harmonization of upconverting nanocrystals and photosensitizer for antimicrobial application. RSC Advances 2015, 5 (124), 102416-102423.